

1 RESEARCH ARTICLE

2 **Antisense transcription from stress-responsive transcription factors**
3 **fine-tunes the cold response in Arabidopsis**

4 **Shiv Kumar Meena^{1,3}, Marti Quevedo^{2, 4}, Sarah Muniz Nardeli², Clément Verez¹,**
5 **Susheel Sagar Bhat¹, Vasiliki Zacharaki¹, Peter Kindgren^{1,*}**

6 ¹Umeå Plant Science Centre, Department of Forest Genetics and Plant Physiology,
7 Swedish University of Agricultural Sciences, 90187 Umeå, Sweden

8 ²Umeå Plant Science Centre, Department of Plant Physiology, Umeå University, 90187
9 Umeå, Sweden

10 ³National Institute of Plant Genome research, Aruna Asaf Ali Marg, New Delhi, 110067,
11 India

12 ⁴Current address: Centre for Research in Agricultural Genomics (CRAG) CSIC-IRTA-
13 UAB-UB, Campus UAB, Bellaterra, 08193, Barcelona, Spain.

14

15 **Short title:** Detection of cold-responsive transcription factors

16

17

18

19 *Corresponding author: Peter Kindgren (peter.kindgren@slu.se)

20 The author responsible for distribution of materials integral to the findings presented in
21 this article in accordance with the policy described in the Instructions for Authors
22 (<https://academic.oup.com/plcell/pages/General-Instructions>) is: Peter Kindgren
23 (peter.kindgren@slu.se)

24 **ABSTRACT**

25 Transcription of antisense long noncoding RNAs (lncRNAs) occurs pervasively across
26 eukaryotic genomes. Only a few antisense lncRNAs have been characterized and
27 shown to control biological processes, albeit with idiosyncratic regulatory mechanisms.
28 Thus, we largely lack knowledge about the general role of antisense transcription in
29 eukaryotic organisms. Here, we characterized genes with antisense transcription
30 initiating close to the Poly(A) signal (PAS genes) in *Arabidopsis* (*Arabidopsis thaliana*).
31 We compared plant native elongation transcript sequencing (plNET-seq) with RNA
32 sequencing (RNA-seq) during short-term cold exposure and detected massive
33 differences between the response in active transcription and steady-state levels of PAS
34 gene-derived mRNAs. The cold-induced expression of transcription factors *B-BOX*
35 *DOMAIN PROTEIN28* (*BBX28*) and *C2H2-TYPE ZINC FINGER FAMILY PROTEIN5*
36 (*ZAT5*) was detected by plNET-seq, while their steady-state level was only slightly
37 altered due to high mRNA turnover. Knockdown of *BBX28* and *ZAT5* or of their
38 respective antisense transcripts severely compromised plant freezing tolerance.
39 Decreased antisense transcript expression levels resulted in a reduced cold response of
40 *BBX28* and *ZAT5*, revealing a positive regulatory role of both antisense transcripts. This
41 study expands the known repertoire of noncoding transcripts. It highlights that native
42 transcription approaches can complement steady state RNA techniques to identify
43 biologically relevant players in stress responses.

44

45

46 **INTRODUCTION**

47 Widespread long non-coding transcription from the complementary DNA (antisense)
48 strand is present at thousands of protein-coding gene loci in eukaryotic organisms.
49 Recent research in plants has evidenced antisense transcription for 30% of expressed
50 genes in the model plant *Arabidopsis* (*Arabidopsis thaliana*) and for 60% of the genes in
51 rice (Chen et al., 2019; Kindgren et al., 2019). Our current understanding is that the
52 majority of antisense transcripts, also called *cis*-natural antisense transcripts (*cis*-NATs),

53 are long non-coding transcripts (>200 nucleotides in length, lncRNA), but their general
54 functional significance remains elusive (Reis and Poirier, 2021). Complementarity
55 between *cis*-NATs and the sense transcript, coupled with the overlapping
56 spatiotemporal expression of sense-antisense pairs, endows them with the potential to
57 engage in the formation double-stranded RNA (dsRNA). dsRNA could undergo
58 subsequent detection by the factors of RNA silencing machinery such as Dicer or Dicer-
59 like (DCL) and Argonaute (AGO) family proteins. However, there is weak evidence that
60 endogenous small interfering RNAs (siRNAs) are derived from NAT-sense pairs (Henz
61 et al., 2007; Reis and Poirier, 2021). Only a handful of studies from different plant
62 species describe a negative role of NATs over the sense transcription (Borsani et al.,
63 2005; Katiyar-Agarwal et al., 2006; Swiezewski et al., 2007; Held et al., 2008; Wan et
64 al., 2016). So far, few *cis*-NATs in plants have been experimentally characterized with
65 mechanistic insights, thereby limiting our understanding of their general function
66 (Wierzbicki et al., 2021). Thus, we only have rudimentary knowledge of the roles of
67 antisense transcription, and its widespread prevalence is certainly an enigma in modern
68 plant research.

69 Our global numerical comprehension of non-coding transcription has been mostly based
70 on sequencing technologies that fundamentally use the steady-state RNA detection
71 principle. For example, in Arabidopsis, 70% of mRNAs were postulated to form sense-
72 antisense pairs based upon RNA-sequencing (RNA-seq) experiments (Wang et al.,
73 2014). However, non-coding transcription is far more pervasive and complex than
74 visualized by canonical steady-state analyses. A major challenge in the field is the
75 detection of antisense and other non-coding transcription due to the low abundance and
76 high turnover rate (Mayer et al., 2015; Kindgren et al., 2019; Thieffry et al., 2020).
77 Classical steady-state level detection methods, such as RNA-seq, are ill-suited to
78 investigate non-coding transcription. In contrast, a technique that investigates active
79 transcription (i.e., Native Elongation Transcript sequencing (NET-seq)) is better suited
80 for detecting rapidly degraded RNA species (Mayer et al., 2015). NET-seq in plants
81 (plaNET-seq or pNET-seq) captures actively transcribing RNA Polymerase II (RNAPII)
82 complexes and enables strand-specific sequencing of the RNA molecules associated
83 with the captured RNAPII complexes before any degradation can occur, thereby

84 uncovering all transcription events genome-wide (Zhu et al., 2018; Kindgren et al.,
85 2019). Case-in-point, plaNET-seq detected ~8,000 unannotated long non-coding
86 transcripts, many of them being antisense transcripts initiating from the host gene's 3'-
87 end (Poly(A) antisense genes, PAS genes) (Kindgren et al., 2019).

88 Emerging evidence indicates that antisense transcription is essential for plant
89 development and stress responses (Matsui et al., 2008; Thieffry et al., 2020). However,
90 the underlying molecular mechanism(s) involved in sense/antisense transcriptional
91 crosstalk often seem idiosyncratic with few common components involved (reviewed in
92 (Lucero et al., 2021)). Nevertheless, antisense RNAs have been characterized to
93 control seed germination (Fedak et al., 2016), phosphate starvation (Jabnour et al.,
94 2013), flowering control (Swiezewski et al., 2007; Henriques et al., 2017), hormonal
95 regulation (Ariel et al., 2020), and cold acclimation (Kindgren et al., 2018). Cold
96 acclimation, initiated by transcriptional processes, allows plants to adapt and eventually
97 withstand freezing. At present cold stress is the sole abiotic stress monitored by
98 plaNET-seq (Kindgren et al., 2019). Remarkably, in plaNET-seq datasets, antisense
99 transcription at PAS genes responds rapidly to cold with a global downregulation,
100 suggesting a putative role in the cold-response (Kindgren et al., 2019). Thus, exposure
101 to cold temperature is an excellent environmental cue for studying antisense
102 transcription's role in Arabidopsis.

103 In this study, we use plaNET-seq and RNA-seq data to show an earlier hidden layer of
104 genes involved in cold acclimation. We show that RNA-seq data poorly captures the
105 cold stress induced transcriptional changes of protein coding genes. On the contrary,
106 plaNET-seq efficiently uncovers these transcriptional changes since transcription is
107 captured prior to their degradation. Among those, we identified two cold-responsive
108 transcription factors that responded natively as crucial for cold acclimation in
109 Arabidopsis. Importantly, experimental validation demonstrated that their antisense
110 transcription is positively correlated to the stress responsiveness of the sense
111 transcription, suggesting a role for antisense transcription in assisting certain
112 transcription factors' stress responses, such as cold exposure.

113

114 RESULTS

115 ***PAS genes are enriched in stress responsive transcription factors with high*** 116 ***active transcription***

117 Genes that host PAS transcription (PAS genes) represent over 3000 genes in
118 Arabidopsis and were recently detected by plaNET-seq (Kindgren et al., 2019). PAS
119 genes are defined as protein coding genes with antisense transcription initiating in the
120 3'-half or 20% of the gene length downstream of the sense gene's PAS (Figure 1A,
121 Supplemental Data Set S1). Characterization of PAS genes has not been done
122 rigorously in Arabidopsis, so we first investigated which biological processes and
123 molecular functions were overrepresented in the list of all PAS genes (Figure 1B-C,
124 Supplemental Data Set S2). Interestingly, there was a clear enrichment of stress-
125 responsive genes that are involved in DNA binding (in particular, transcription factors
126 (TFs)). Therefore, for our further analysis, we decided to divide the PAS genes into PAS
127 TFs ($n = 294$) and PAS non-TFs. We also included TFs without PAS (TFs non-PAS) as
128 a control group. An example of a known stress-responsive gene encoding a TF with an
129 antisense transcript that responds natively to cold temperature was *WRKY48* ((Xing et
130 al., 2008), Figure 1D).

131 Overall, PAS genes tended to be shorter than other expressed genes and TFs
132 non-PAS (Figure 2A) and the steady-state levels of PAS non-TFs or PAS TFs gene
133 mRNA were not significantly different from those of all expressed genes (Figure 2B).
134 Surprisingly, PAS gene mRNA had a greater turnover rate compared to all expressed
135 genes when measured by RNA-seq after treatment with the transcription inhibitor,
136 cordycepin (alpha decay) (Figure 2C) (Sorenson et al., 2018). TFs non-PAS also
137 showed a significantly higher turnover rate, suggesting that the rapid degradation of
138 mRNA in these classes of genes are independent of antisense transcription. We
139 confirmed these results with data from transcription inhibition with another inhibitor,
140 actinomycin D (Supplemental Figure S1A) (Narsai et al., 2007). Both PAS non-TFs and
141 PAS TFs genes displayed high active RNAPII transcription at the genome-wide level
142 compared to expressed genes and TFs non-PAS (Figure 2D, Supplemental Figure
143 S1B). In addition, PAS-TFs showed a higher RNAPII occupancy compared to PAS non-

144 TFs (Supplemental Figure S1B). Thus, the higher expression level of PAS genes and
145 high turnover rate explained the small effects on RNA steady state-levels. Taken
146 together, PAS genes are enriched in stress responsive transcription factors with high
147 transcriptional and post-transcriptional regulation. Moreover, the high turnover rate
148 seems to be a general feature of TF mRNAs and not a consequence of PAS TF
149 antisense transcription.

150 ***The expression levels of cold responsive genes detected by plaNET-seq correlate***
151 ***poorly with RNA-seq***

152 The high transcription activity of PAS genes and rapid turnover of their mRNA made us
153 interested in comparing the genome-wide steady state levels of mRNA to how genes
154 are actively transcribed (plaNET-seq). Thus, we performed RNA-seq using samples
155 from seedlings grown similarly to the plaNET-seq experiment (10 days in long day
156 conditions at 22°C and cold stress samples from 3h at 4°C and 12 h at 4°C). In our cold-
157 treated RNA-seq dataset, many mRNAs drastically changed their steady-state level
158 (Figure 3A, Supplemental Data Set S3). When we compared DE genes (fold change)
159 between our RNA-seq and plaNET-seq datasets, we saw that RNA-seq poorly reflected
160 the genes differentially expressed determined by plaNET-seq (Kindgren et al., 2019).
161 The overlap was only 616 of the up-regulated (UP) genes and 270 of the down-
162 regulated (DOWN) genes in the same direction after 3h at 4°C (Figure 3A). After 12h at
163 4°C, we observed increased overlap, 1819 of UP genes and 1674 of DOWN genes
164 (Figure 3A). In addition, we saw a low correlation between the DE gene fold change at
165 both time points (Figure 3B-C). This suggests that there is a clear discrepancy between
166 the active transcriptional changes (plaNET-seq) and changes to the steady-state levels
167 of mRNA (RNA-seq) occurring during cold stress, especially early in the cold response.

168 Focusing on the PAS genes, we saw a similar pattern as in all DE genes (Figure
169 3D-F). Astoundingly, we found that 2214 (71%) PAS genes changed their expression
170 significantly to cold (either in plaNET-seq or RNA-seq data) at one or both cold time
171 points, corroborating their responsiveness to stress (Supplemental Data Set S4). Out of
172 these genes, 229 were PAS TFs (78% were responsive to cold, Supplemental Data Set
173 S4). To further confirm that PAS genes are highly responsive to cold, we compared

174 PAS genes UP after 3h 4°C with UP genes without antisense transcription (determined
175 by plaNET-seq). At 22°C, PAS genes showed an increased RNAPII stalling around the
176 +1 nucleosome, a hallmark for stress-responsiveness compared to other UP and non-
177 DE genes (Figure 4A) and an overall high active transcription (Figure 4B). After 3h 4°C,
178 PAS UP genes showed a more extreme response to cold temperature compared to
179 other UP genes (Figure 4C-D), suggesting that, indeed, PAS genes have an enhanced
180 responsiveness to cold compared to other genes. In contrast, antisense transcription for
181 upregulated PAS genes remained similar throughout the cold response (Supplemental
182 Figure S2). Taken together, these data strengthen the hypothesis that PAS genes are
183 inclined to respond to cold temperatures, but there is no correlation between PAS host
184 gene expression and antisense expression during the initial cold response. In addition,
185 the discrepancy between plaNET-seq and RNA-seq argues that some transcription
186 factors might have been overlooked as cold-responsive genes and highlight the use of
187 combining nascent RNA methods with steady-state levels of mRNA to fully understand
188 the cold response in an organism.

189 ***The discrepancy between active transcription and steady state levels can partly***
190 ***be explained by mRNA turnover rates***

191 Next, we focused on the differentially expressed TFs with antisense transcription. We
192 aimed to identify additional biologically important TFs in the cold response. A special
193 emphasis was put on the expression pattern in plaNET-seq as the distinct dynamics of
194 PAS TFs mRNAs (Figure 2) might have masked cold responsive TFs in earlier studies.
195 We reasoned that rapidly responsive TFs had a high probability to be involved in cold
196 acclimation since this expression pattern mirrors that of known assigned TFs in the cold
197 response, such as C-REPEAT BINDING FACTOR2 (CBF2, At4g25470) (Figure 5A).
198 CBF2 is massively induced and transiently peaks after 3h at 4°C. Out of the 242 PAS
199 TFs that responded to cold, 25 showed a similar plaNET-seq expression pattern to
200 CBF2 (UP after 3h and DOWN between 3 and 12h) (Supplemental Data Set S5). Only 9
201 of the 25 genes showed up-regulation by RNA-seq after 3h (Supplemental Data Set
202 S5). An example of a gene that was DE in plaNET-seq but not in RNA-seq was HY5-
203 HOMOLOG (HYH, At3g17609) (Figure 5B).

204 Due to the RNA degradation characteristics of PAS TFs, we first tested the
205 mRNA turnover rates (by cordycepin incubation) for 5 randomly chosen genes from the
206 25 genes with convincing expression patterns in plaNET-seq and no or slight
207 upregulation by RNA-seq. MYB DOMAIN PROTEIN-47 (MYB47, At1g18710) has a
208 potential role in drought and hormone signaling (Ding et al., 2014; Marquis et al., 2022).
209 CONSTANS-LIKE 7 (COL7, At1g73870) is involved in the shade avoidance response
210 (Wang et al., 2013). The C2H2-type zinc finger family protein, *C2H2-TYPE ZINC*
211 *FINGER FAMILY PROTEIN-5* (ZAT5, At2g28200) and SCARECROW-LIKE-8 (SCL8,
212 At5g52510), are uncharacterized proteins and B-BOX DOMAIN PROTEIN-28, (BBX28,
213 At4g27310) has been characterized for its involvement in flowering and
214 photomorphogenesis (Song et al., 2020; Cao et al., 2022). *MYB47*, *SCL8*, and *BBX28*
215 showed a slight up-regulation in the RNA-seq data. However, neither BBX28, SCL8,
216 MYB47 or any of the other chosen proteins have a known function in the cold response
217 of Arabidopsis. Our assay control *EUKARYOTIC TRANSLATION INITIATION*
218 *FACTOR-4A1* (*EIF4A1*), a stable mRNA at 22°C, showed similar stability at 4°C as
219 compared to 22°C (Figure 5C). In addition, a recent study showed increased stability in
220 cold for a key TF in the cold response, *CBF1* (Zacharaki et al., 2023). In contrast, all the
221 PAS TF candidate genes' mRNAs, except *SCL8*, showed a significantly decreased
222 transcript stability at 4°C compared to 22°C (Figure 5D-H). Thus, induced transcriptional
223 activity at gene loci responding to cold may remain partly undetected by steady state
224 methods due to rapid mRNA decay at 4°C. Again, our results highlight that nascent
225 transcription methods can complement RNA steady state level methods to identify
226 stress responsive genes, in particular those with highly dynamic regulation and mRNA
227 turnover.

228 **ZAT5 and BBX28 are involved in cold acclimation**

229 Can mRNAs with minor differences in steady state levels during stress have an
230 important biological role in the stress adaptation for the plant? To answer this, we
231 focused on two candidate genes for our continued analysis, *ZAT5* and *BBX28*. Both
232 genes responded rapidly to cold temperatures, as detected by plaNET-seq (Figure 6A-
233 B). We could not detect any significantly increased steady-state level of *ZAT5* after

234 exposure to 4°C with RT-qPCR, although a positive trend was observed early in the
235 cold response (Figure 7A). We did see a significant down-regulation from control levels
236 starting at 8 h of 4°C (Figure 7A). For *BBX28*, we could not detect any significant up- or
237 down-regulation, but a positive trend early in the cold response was observed (Figure
238 7B). The discrepancy between our RT-qPCR and RNA-seq results may suggest that the
239 up-regulation of *BBX28* and *ZAT5* is slight and not always consistently statistically
240 significant depending on separate cold treatments and the variation between replicates.
241 However, since both *BBX28* and *ZAT5* have been found to be diurnally expressed
242 (Romanowski et al., 2020), we also checked their steady state levels with controls
243 (seedlings kept at 22°C) taken at the same time points as the cold samples (3h and 12
244 at 4°C). Here, we did see a small but significant increase of both *BBX28* and *ZAT5* after
245 3h (Supplemental Figure S3A-B).

246 To test their biological importance in the cold acclimation process, we isolated
247 two independent T-DNA lines disrupting the two genes and subjected these lines to a
248 freezing test together with wild type (Figure 7C-D). In the freezing test, leaf discs of non-
249 acclimated and cold-acclimated plants (4 days in 4°C) are in contact with water and
250 exposed to decreasing freezing temperatures and measured for plasma membrane
251 disruption (i.e., leakage of electrolytes). Therefore, measuring electrolyte leakage is a
252 measurement of how well the cells can survive freezing temperatures. Indeed, we found
253 that both mutant lines were impaired in their acclimation to cold. For *zat5-1*, the freezing
254 tolerance was significantly lower ($-3.7 \pm 1.7^\circ\text{C}$, $p < 0.0001$) compared to $-6.1 \pm 0.2^\circ\text{C}$ for
255 WT. The freezing tolerance for *bbx28-1* was also significantly lower ($-5.7 \pm 0.2^\circ\text{C}$,
256 $p = 0.0022$) compared to $-6.5 \pm 0.2^\circ\text{C}$ for WT. We could not detect any difference in non-
257 acclimated plants (Supplemental Figure S3C-D), suggesting that both *ZAT5* and *BBX28*
258 have a specific role in the cold acclimation process in Arabidopsis. Overall, these results
259 indicate that changes to the transcription activity with minor changes to the mRNA
260 steady state levels can have a significant biological role.

261 ***Antisense transcription is required for proper regulation of ZAT5 and BBX28***

262 Next, we turned to our second question; what is the role of antisense transcription along
263 the *ZAT5* and *BBX28* gene body? Our plaNET-seq data revealed that both *ZAT5* and

264 *BBX28* had antisense transcription affected by cold temperature, although the
265 differences were small compared to sense expression (Figure 8A-B, upper panel). To
266 identify the 5' and 3'-end of *asZAT5* and *asBBX28*, we used available Cap Analysis of
267 Gene Expression sequencing (CAGE) (Thieffry et al., 2020) and Direct RNA
268 Sequencing (DRS) data (Schurch et al., 2014) (Figure 8A-B, middle and lower panels).
269 Interestingly, both antisense transcripts are targets of the nuclear exosome (see CAGE
270 data for the exosome mutants *hen2-2* and *rrp4-2*). Consequently, 5'-ends are more
271 prominent in the exosome mutants, suggesting that the transcripts are degraded rapidly
272 after their synthesis. We could see that there was no precise start or end to the
273 antisense transcription, but rather a window at both ends. Antisense transcription starts
274 well beyond the poly(A)-site of their host genes and navigates until at least 1 kb
275 upstream of the host gene's transcription start site (TSS).

276 To investigate the role of the antisense transcription at the translational level,
277 firefly luciferase (*LUC*) reporter constructs for *ZAT5* were generated, using GreenGate
278 cloning system (Lampropoulos et al., 2013), with and without the 1403 bp DNA
279 sequence that harbors *ZAT5* 3' UTR, associated PAS antisense transcript and putative
280 promoter i.e. *ProZAT5:ZAT5-LUC-UTR-ASProZAT5* and *ProZAT5:ZAT5-LUC-tNOS*.
281 The *Agrobacterium tumefaciens* cultures carrying these plasmids were used for
282 infiltration of *Nicotiana benthamiana* leaves for transient expression assay
283 (Supplemental Figure S4A-B). The first construct included the endogenous promoter
284 and cDNA fused to the *LUC* gene. Downstream of the *LUC* gene was the endogenous
285 untranslated 5'-region of *ZAT5* and the AS promoter. In the second construct, the *ZAT5*
286 promoter and cDNA were fused to *LUC* followed by the strong tNOS terminator. The
287 tNOS terminator diminishes any antisense transcription over the *LUC* and *ZAT5* gene
288 body (Kindgren et al., 2018). The endogenous construct (construct 1 in Supplemental
289 Figure S4) showed an induction after cold exposure, confirming that the *ZAT5* promoter
290 is cold responsive and corresponds with positive transcriptional regulation of *ZAT5* by
291 its antisense (Supplemental Figure S4C). At both 22°C and 4°C, the tNOS construct
292 showed lower *LUC* activity compared to the full-length construct (Supplemental Figure
293 S4D-E). The overall cold responsiveness decreased from 2.5-fold in the full-length
294 construct to 2.0-fold in the tNOS construct, suggesting that the antisense transcription

295 over *ZAT5* has a positive role for the transcription level and stress responsiveness of
296 the gene.

297 To further elaborate their role, the promoter region of the antisense transcription
298 was targeted with the CRISPR-Cas9 approach to minimally alter and knockout only
299 parts of their regulatory sequence and/or the 5'-end of the TSS window. That way, the
300 direct interference with sense transcription would be minimized. For *ZAT5*, we were
301 able to retrieve a mutant with a 283 bp deletion i.e. 392 bp from the start of the TSS
302 window of *asZAT5* and 710 bp from the poly(A) site for *ZAT5* (Figure 9A). We named
303 this mutant *aszat5-1*. For *BBX28*, we aimed to delete the 5'-end of the TSS window of
304 *asBBX28*. We retrieved a 392 bp deletion that included a deletion of 220 bp of the TSS
305 window (*asbbx28-1*, Figure 9A). The deletion is 193 bp from the poly(A) site of sense
306 *BBX28*. In both mutants, we did not alter the stability of the respective mRNA,
307 suggesting that we did not interfere with transcription termination (Supplemental Figure
308 S5A-B).

309 In *aszat5-1*, there was a significant down-regulation of the nascent transcription
310 of *asZAT5* at 22°C but we could not detect any difference after 3h 4°C (Figure 9B). For
311 *ZAT5*, the mutant showed lower nascent transcription at both time points (Figure 9B).
312 The steady-state levels of *ZAT5* showed a decreased level after cold treatment (Figure
313 9B). These results corroborate the results from the *ZAT5* constructs and suggests two
314 key regulatory aspects, antisense transcription over the *ZAT5* locus is required for
315 proper cold induction and that CRISPR-Cas9 targeted *asZAT5* promoter sequences
316 contain regulatory elements in the antisense promoter to regulate the initiation of
317 *asZAT5* transcription. To show a biological role for *asZAT5*, we performed cold
318 acclimation and freezing test in the *aszat5-1* mutant (Figure 9C). We found a
319 significantly lower freezing tolerance for the *aszat5-1* ($-4.8 \pm 0.2^\circ\text{C}$, $p=0.0021$) compared
320 to WT ($-5.9 \pm 0.2^\circ\text{C}$). In *asbbx28-1*, we detected a significant down-regulation of the
321 nascent transcription of *asBBX28* at 22°C and lower active transcription of *BBX28* at
322 both 22°C and 3h 4°C (Figure 9D). The steady state level of the sense *BBX28* transcript
323 was also lower in this mutant (Figure 9D), corroborating that antisense transcription had
324 a positive role on sense *BBX28* transcription as it had on *ZAT5* transcription.

325 Additionally, we could see a significant decrease in the freezing tolerance in the mutant
326 ($-4.0 \pm 1.1^\circ\text{C}$, $p=0.0015$ for *asbbx28-1* and $-5.9 \pm 0.2^\circ\text{C}$ for WT, Figure 9E).

327 Our results suggest that antisense transcription of *ZAT5* and *BBX28* has a
328 positive role in priming the sense transcription for stress response and that the
329 characterized antisense transcription has an important biological role in the cold
330 acclimation process. All in all, our study shows that antisense transcription can play a
331 crucial role in priming certain plant stress-responsive transcription factors.

332

333 DISCUSSION

334 A remarkable finding in our study is that the nascent transcriptional response to cold
335 differs from the one detected by steady-state level measurements (Figure 3).
336 Additionally, we show that plaNET-seq complements steady-state methods (RNA-seq)
337 to detect genome-wide transcriptional changes in the cold response (Figure 3). A similar
338 concept has earlier been proposed for heat stress in *Arabidopsis* (Liu et al., 2021).
339 Thus, these reports highlight the importance of taking into account both active
340 transcription and steady state levels of mRNA to fully understand the response to stress
341 (Sidaway-Lee et al., 2014). Changes in the active transcription of a gene measured by
342 plaNET-seq have biological relevance, even though the steady-state level of the gene's
343 mRNA is only slightly different to control conditions after cold exposure (Figure 4-5).
344 This report takes active transcription into account to find cold responsive genes in
345 *Arabidopsis*.

346 This study characterizes genes with antisense transcription that initiates from the 3'-end
347 of genes in *Arabidopsis* (Figure 1-2). Notably, we find a stark contrast in how the
348 *Arabidopsis* genome implicates antisense transcription compared to other eukaryotes.
349 In human cells, antisense transcription is most prevalent from early exon-intron
350 junctions of genes (Brown et al., 2018). This type of antisense transcription is generally
351 associated with low active transcription (Mayer et al., 2015), albeit with higher stability of
352 the sense transcript (Brown et al., 2018). In *Arabidopsis*, we see almost the opposite
353 scenario. Antisense transcription is most prevalent from the 3'-end of genes and their

354 host genes are associated with high active transcription and fast turnover rates (Figure
355 2) (Kindgren et al., 2019). In agreement, accelerated transcript degradation is
356 suggested as an advantageous evolutionary strategy to facilitate genome wide swift
357 responses during cold stress in Arabidopsis (Chiba et al., 2012). It is likely that plants,
358 being sessile organisms, have evolved distinct ways of gene regulation compared to
359 other eukaryotes, especially when responding to biotic and abiotic stresses. This
360 hypothesis is corroborated by the fact that many genes with antisense transcription in
361 Arabidopsis are stress-regulated transcription factors (Figure 1), proteins that are
362 required to kick-start stress responses.

363 Our data paints a picture of how plants keep their stress-responsive transcription
364 factors in a constant “on” mode to prime their response to stress situations. A tempting
365 hypothesis would be that antisense transcription is involved in sense transcript
366 degradation, a generalized regulatory role that was widely postulated for several
367 thousands of NATs in Arabidopsis and other plant species (Borsani et al., 2005; Held et
368 al., 2008). However, our data does not endorse the concept of ‘universal gene silencing
369 roles of NATs’ but rather indicates that antisense transcription could have a more
370 positive regulatory role on sense transcription (Reis and Poirier, 2021). When antisense
371 transcription is down-regulated after cold exposure (Figure 6, Supplementary Figure 2),
372 sense transcript stability is lower compared to 22°C (Figure 5) and in our CRISPR-Cas9
373 deletion lines that exhibit reduced antisense transcription, we detected decreased sense
374 mRNA levels at 4°C (Figure 9). In addition, our data from *ZAT5* and *BBX28* highlight
375 that even a marginal reduction of their antisense transcription can impair the cold
376 responsiveness and ability of plants to acclimate to cold temperatures (Figure 9).

377 Thus, an outstanding question and an important avenue for future research is how
378 antisense transcription could relay a positive role to mRNA steady-state levels. A
379 possible mechanism could be that the antisense transcription increases the stability of
380 the sense transcript and assists in the translation of the sense transcript, as shown for
381 the rice lncRNA, *cis-NAT PHOSPHATE1;2* (*cis-NAT PHO1;2*) (Jabnoue et al., 2013).
382 However, this is unlikely to be a general mechanism since most antisense transcripts
383 are short lived and degraded soon after their synthesis (Figure 8) (Kindgren et al., 2019;

384 Thieffry et al., 2020) and in our CRISPR lines, we did not see any effect of the mRNA
385 stability (Supplemental Figure S5). Another, more likely mechanism, could be
386 antisense-promoted changes to the local chromatin environment which could be
387 important in priming the optimal transcriptional response, resembling the example of
388 *NUCLEAR ENRICHED ABUNDANT TRANSCRIPT 1 (NEAT1)* lncRNA in animals
389 where the act of transcription itself at the *NEAT1* locus was shown to be sufficient for
390 biological function (Mao et al., 2011). It is possible that sense-antisense promoters can
391 act autonomously both during developmental transitions and in stress conditions if
392 uncoupled from the genomic context of each other, as shown for e.g., *asDOG1*,
393 *COOLAIR* and *SVALKKA* (Swiezewski et al., 2009; Fedak et al., 2016; Kindgren et al.,
394 2018). In contrast, the strong influence of native antisense transcription in *cis* over *ZAT5*
395 and *BBX28* suggests that genomic proximity of the sense-antisense pairs could be
396 crucial for the cold acclimation process (Figure 9). In fact, genome-wide native
397 transcriptional analysis in *Saccharomyces cerevisiae* reinforces the idea that the
398 dynamic chromatin structures could be central in determining the landscape of
399 eukaryotic sense-antisense transcription (Murray et al., 2015).

400 In Arabidopsis, the H3K27 demethylase *RELATIVE OF EARLY FLOWERING-6*
401 (*REF6*) has been proposed to recruit a chromatin remodeling complex that includes
402 *BRAHMA* to regulate antisense transcription (Li et al., 2016; Archacki et al., 2017).
403 Other repressing chromatin mechanisms have been described for *COOLAIR*,
404 *AGAMOUS INTRONIC RNA-4 (AG-incRNA4)*, and *AUXIN PROMOTER REGULATED*
405 *LOOP (APOLO)*, albeit their mechanisms of action are distinct (Ariel et al., 2014;
406 Csorba et al., 2014; Wu et al., 2018; Ariel et al., 2020). In a parallel manner, it is
407 possible for lncRNAs to mediate deposition of activating marks in histones by recruiting
408 other sets of modifiers, as has been shown for the antisense transcript of *MADS*
409 *AFFECTING FLOWERING 4 (MAF4)* and *MARNERAL SILENCING (MARS)* in
410 Arabidopsis (Zhao et al., 2018; Roulé et al., 2022). Similar modes of action have been
411 reported in other plant species as well for example an antisense lncRNA, transcribed
412 from *DgTCP1 (CLASS I TEOSINTE BRANCHED1/CYCLOIDEA/PROLIFERATING*
413 *[TCP] transcription factor)*, arbitrates histone modification depositions at the sense
414 promoters playing a positive role in cold tolerance in *Chrysanthemum morifolium* (Li et

415 al., 2022). It will be central to focus on different histone marks and histone variants in
416 future studies of antisense genes to elucidate noncoding transcription and its broader
417 role(s) in plants.

418 Our discoveries take the first steps to a broader role of antisense transcription in plants
419 and support the notion that transcription from the complementary strand modulates the
420 responsiveness of stress genes. Furthermore, our study moves away from the paradigm
421 that antisense transcription has a prominent silencing role in plants instead supporting a
422 more positive regulatory function.

423

424 **MATERIALS AND METHODS**

425 **Plant growth, mutants and CRISPR-Cas9 mutant generation**

426 For the wild-type background *Arabidopsis* (*Arabidopsis thaliana*) *Col-0* or Columbia
427 accession was employed. For the growth of plants, seeds were surface sterilized and
428 stratified for 2-4 days at 4° C in the dark and either transferred to soil directly or plated
429 on ½ Murashige and Skoog (MS) basal medium supplemented with 1% (w/v) sucrose.
430 Plants were grown in long day conditions (16h light, 8 dark, ~100 µE, SciWhite LEDs
431 (Percival)) for 10 days. Biological replicates in all experiments represent approximately
432 20-30 seedlings grown on separate plates. Cold treatment (4° C, ~25 µE) was initiated
433 at ZT4 to replicate the conditions set by the plaNET-seq dataset. T-DNA insertional
434 mutant lines viz: *zat5-1* (*SALK_041934*), *bbx28-1* (*SAIL_412_A09*), *hen2-2*
435 (*GABI_774H07*, (*Lange et al., 2014*)) were genotyped and confirmed for homozygosity
436 by PCR. For the CRISPR-Cas9 mutants, guide RNAs (gRNAs) were designed using the
437 CHOPCHOP webserver (<http://chopchop.cbu.uib.no/>) and a 2gRNA fragment was
438 amplified using DT1T2 plasmid (Xing et al., 2014) template using Phusion DNA
439 polymerase (Thermo Fisher Scientific). Oligos used can be found in Supplementary
440 Data Set 6. The PCR product was electrophoresed, and gel purified followed by Green
441 Gate reaction into a modified pHSE401 binary vector as described before (Xing et al.,
442 2014). In the modified pHSE401 vector, the hygromycin resistance has been replaced
443 by a *GFP* seed coat expression cassette for faster screening. Final plasmids were

444 verified by sequencing and transformed into wild type *Col-0* plants by *Agrobacterium*
445 *tumefaciens* (GV3101) floral dip. T1 seeds were first selected by visual screening for
446 *GFP* expression followed by PCR genotyping. Further selection of the T2 lines was
447 performed by picking seeds lacking the GFP signal, and then homozygous plants were
448 confirmed by PCR for the genomic deletion and the absence of the Cas9 construct.
449 Seeds from homozygous plants were used in experiments.

450 **Generation of reporter constructs**

451 We used GreenGate cloning system for generation of firefly luciferase (LUC) gene
452 reporter constructs (Lampropoulos et al., 2013). To construct *ProZAT5:ZAT5-LUC-UTR-*
453 *ASProZAT5* and *ProZAT5:ZAT5-LUC-tNOS*, 2438 bp fragment upstream (1408 bp
454 promoter and 1030 CDS of *ZAT5* without stop codon) was PCR amplified from genomic
455 DNA . A separate PCR amplification was carried out for 1402 bp long *UTR-ASZAT5_{prom}*
456 fragment using proofreading Phusion DNA polymerase using genomic DNA template.
457 LUC and tNOS terminator (tNOS) were also separately PCR amplified in similar
458 manner. Subsequently different PCR products were cloned into respective GreenGate
459 entry modules by employing Bsal/T4 DNA ligase and using reaction conditions as
460 described earlier (Lampropoulos et al., 2013). All Greengate entry plasmids were
461 confirmed by restriction digestion and DNA sequencing. Finally, the GreenGate reaction
462 was performed for the assembly of 6 entry modules to create final destination plasmids
463 i.e. *ProZAT5:ZAT5-LUC-UTR-ASProZAT5* and *ProZAT5:ZAT5-LUC-tNOS* using
464 pGGZ003 as backbone vector according to protocol reported earlier (Lampropoulos et
465 al., 2013). Oligos used can be found in Supplemental Data Set S6.

466 **Transient agroinfiltration and luciferase assay**

467 *Agrobacterium* strain GV3101 was separately transformed with plasmids harboring
468 *promZAT5::ZAT5-LUC-UTR-ASZAT5_{prom}* and *promZAT5::ZAT5-LUC-tNOS* constructs and
469 plated on LB media containing 10 µg/ml rifampicin, 25 µg/ml gentamicin, 75 µg/ml
470 spectinomycin. After 48 hours of growth positive colonies selected and grown in 5 ml of
471 LB medium supplemented with antibiotics. Additionally, presence of constructs in
472 *Agrobacteria* confirmed by colony PCR. After overnight growth at 30°C, 30 ml of fresh
473 induction media (LB supplemented with 10 mM MES pH 5.6, 20 µM acetosyringone, 25

474 $\mu\text{g/ml}$, gentamicin, 75 $\mu\text{g/ml}$ spectinomycin, 10 $\mu\text{g} / \text{ml}$ rifampicin) inoculated. When
475 OD_{600} reached 0.5, cells were harvested by centrifugation and resuspended in
476 infiltration media (LB supplemented with 10 mM MES pH 5.6, 10 mM MgCl_2 and 150
477 μM acetosyringone without antibiotics) to obtain an OD_{600} value of 1 followed by
478 incubation of bacterial culture at room temperature for minimum of 3 hours. Finally,
479 leaves from 6-week-old *N. benthamiana* plants were infiltrated with bacterial suspension
480 and the area was delimited and marked with a marker.

481 72 hours post agroinfiltration, half of the randomly selected *N. benthamiana* plants (a
482 minimum of 5 independent plants each with 2-3 infiltrated leaves for individual
483 constructs) were subjected for cold stress treatment (3h cold 4°C) at ZT4. Control plants
484 were maintained at 22°C . Immediately after 3 hours of cold stress, previously infiltrated
485 leaves with marked area from cold treated and control plants were carefully and quickly
486 re-infiltrated with 5 mM working solution of D-Luciferin (GoldBio®). The ratio of 5mM D-
487 Luciferin in 0.01% (v/v) triton X100 and sterile water was kept at 1:3 during re-infiltration
488 of leaves. Further, several 1 cm leaf discs were prepared from marked re-infiltrated area
489 and subjected for luminescence measurement after 5-10 minutes of incubation at
490 respective temperatures by GloMax® Navigator Microplate Luminometer. Data
491 extracted and analyzed using Excel and GraphPad® software.

492 **Electrolyte leakage assay**

493 Electrolyte leakage measurements were carried out according to previous report
494 (Kindgren et al., 2015). In short, plants were grown in short days (8h light /16 h dark
495 cycle) for 4 weeks. For the cold acclimation experiments, WT and mutant plants were
496 transferred to a cold chamber set at 4°C for 4 days without changing photoperiodic
497 conditions. Randomized leaf discs of 1 cm diameter, for each genotype in triplicates
498 from several similar sized leaves, were prepared using a cork borer for acclimated or
499 non-acclimated plants and carefully placed horizontally in a manner to avoid floating in
500 clean glass tubes filled with 200 μl deionized distilled water. The tubes containing two
501 leaf discs were then transferred to a programmable freezing bath (FP51, Julabo,
502 Germany) set at -2°C . After 45 minutes, icing was induced manually in each tube with
503 the help of liquid N_2 and a metallic stick. Temperature decrease occurred at the rate of

504 -1°C per 30 mins, and samples were taken out at designated temperature point(s)
505 followed by incubation on ice for at least 1 hour in the cold room (4°C). Soon after the
506 collection and 1 hour ice-incubation of tubes, 1.3 ml of water was added to each tube
507 and placed on a shaker overnight at 4°C and conductivity was measured using a
508 conductivity cell (CDM210, Radiometer, Denmark) on the next day. Finally, all tubes
509 were subjected to flash freeze using liquid N_2 and left on a shaker overnight at room
510 temperature. To obtain the total electrolyte content from leaf discs, conductivity was
511 measured again, and the % of electrolyte leakage was calculated using the formula –
512 (conductivity before flash freeze/ conductivity after flash freeze) *100. Data were fitted
513 into a sigmoidal dose-response curve using GraphPad Prism software and significant
514 differences of the fit were determined with an extra sum-of-squares F test.

515 **RNA extraction, cDNA synthesis and RT-qPCR**

516 Total RNA extraction from plant material was carried out using RNeasy Plant Mini Kit
517 (QIAGEN) as per suppliers' instructions. The extracted RNA was additionally treated
518 with dsDNase (Thermo Fisher Scientific) for the elimination of genomic DNA
519 contamination. Successively, complementary DNA (cDNA) synthesis was carried out
520 using Superscript IV® (Invitrogen) reverse transcriptase as per manufacturer
521 instructions using strand-specific RT primers carrying a sequence tag
522 (GACTGGAGCACGAGGACACT) at 5' end (Parent et al., 2015; Kindgren et al., 2018)
523 together with a reference gene. Quantitative real-time PCR (RT-qPCR) was performed
524 on CFX96 and CFX384 Real-Time PCR detection systems (BioRad) using SYBR
525 premix (Bio-Rad), cDNA, reverse primer (aligning to tag sequence) and appropriate
526 forward primers at the concentration of $10\text{ pmol}/\mu\text{l}$ with the PCR cycler following initial
527 denaturation at 95°C for 30s, standard 40 cycles of 94°C for 10 s, 60°C for 30s. The
528 specificity of RT-qPCR products was assessed from the single peak melt curves. For
529 the data analysis, the C_q values from a minimum of 3 biological replicates with 2-3
530 technical replicates were averaged and ΔC_q was obtained as C_q (gene of interest)- C_q
531 (reference gene). Final calculations were performed by following with $2^{(-\Delta C_q)}$ or $2^{(-\Delta\Delta C_q)}$,
532 adjusted to experimentally determined primer efficiency for determination of fold change

533 in gene expression levels. Statistical significant differences were calculated with
534 Student's t-test. Primers used are listed in Supplemental Data Set S6.

535 **Measuring nascent transcription**

536 Nuclei were isolated from around 3 grams of 12-day old seedlings with Honda buffer
537 (0.44 M Sucrose, 1.25% Ficoll, 2.5% Dextran T40, 20 mM Tris –HCl pH 7.4, 10 mM
538 MgCl₂, 0.5% Triton-X, Prot. inhibitor tablet, RNase inhibitor, 5 mM DTT). The nuclear
539 lysis and RNAPII-IP were done according to (Kindgren et al., 2018) with small
540 modifications. Briefly, after lysis and DNase I treatment, the supernatant was mixed with
541 protein G magnetic beads (Thermo Scientific) coupled to an endogenous RNAPII
542 antibody (8WG16, Sigma Aldrich) for 2h in 4°C. The beads were washed 4 times with
543 wash buffer (0.3 M NaCl, 20 mM Tris-HCl pH 7.5, 5 mM MgCl₂, 5 mM DTT, proteinase
544 inhibitor tablet and RNase inhibitor (20 U/ml)). To disrupt the RNAPII complexes, QIAzol
545 was added, and RNA was isolated using the miRNeasy kit from Qiagen. RNA
546 concentration was measured with Nanodrop and approximately 100 ng was used for
547 cDNA synthesis with gene specific primers and Superscript IV (Invitrogen) according to
548 manufacturer's instructions. Oligos used can be found in Supplemental Data Set S6.

549 **RNA sequencing and analysis**

550 RNA was isolated from 10-day old Arabidopsis Col-0 seedlings grown on ½MS medium.
551 Briefly, seeds were stratified for 2-4 days at 4°C in the dark, followed by growth in long
552 day (16h light/8h dark, 22°C Day/18°C night) conditions and ~100μEm⁻²s⁻¹ light. On the
553 12th day, seedlings were subjected to cold stress (4°C) for 3h and 12h with ~20-25μEm⁻²
554 s⁻¹ light. Total RNA was isolated using RNeasy Plant Mini Kit (QIAGEN) according to
555 manufacturer's instructions. RNA thus obtained was treated with TURBO® DNase
556 (Thermo Fischer) according to the standard protocol. Three biological replicates from
557 each time point of RNA samples were sent to Novogene Europe where strand specific
558 libraries were prepared and sequenced using Illumina's NovaSeq 6000 platform.
559 Libraries were sequenced to a depth of 40-60 million raw reads (6G raw data per
560 sample). For data analysis, the guidelines previously established at UPSC were
561 followed (Delhomme et al., 2023). Pre-processing of data was done using FastQC
562 v0.11.9 (quality control of the raw data) and SortMeRNA v4.3.4 ((Kopylova et al., 2012);

563 filter and remove rRNA contamination). Thereafter, Trimmomatic v0.32 (Bolger et al.,
564 2014) was used to trim the adapter sequences and FastQC was performed again to
565 ensure data integrity. Salmon v1.6.0 (Patro et al., 2017) was used to determine the read
566 counts with ARAPORT11 as a reference. R-package DESeq2 (Love et al., 2014) was
567 used to perform the differential expression analysis. Statistically significant genes were
568 filtered using the following parameter: false discovery rate (fdr) < 0.05 and log₂ fold
569 change ≥ 0.5. RNA-seq data have been deposited on GEO (GSE252832). To
570 investigate the rate of transcript degradation of control genes vs PAS-host genes we
571 used the Decay Rate (alpha estimate) from Sorenson RS and Deshotel MJ et al (Table
572 S2 from cited paper) (Sorenson et al., 2018), which was originally determined by
573 cordycepin treatment followed by RNA-seq. In addition, we used available data to
574 estimate the decay rate for mRNAs after actinomycin D treatment (Narsai et al., 2007).
575 GO-term enrichment was done at TAIR
576 (https://www.arabidopsis.org/tools/go_term_enrichment.jsp).

577 **RNA stability assay**

578 RNA stability measurements to determine the half-life ($t_{1/2}$) of transcripts were
579 performed according to previous report (Fedak et al., 2016). In summary, 10 days old
580 wild-type seedlings were grown in long day photoperiod (16h light/8h dark, 22°C
581 Day/18°C night) (CLF Plant Climatics cabinet) over ½ MS medium supplemented with
582 1% sucrose (w/v). On day 10, seedlings were transferred to liquid ½ MS media and
583 acclimatized while maintaining 22°C or 4°C growth temperatures for respective sample
584 sets under the same light conditions. Further, samples from 22°C or 4°C were
585 transferred to incubation buffer (1 mM PIPES at pH 6.25, 1 mM trisodium citrate, 1 mM
586 KCl and 15 mM sucrose) in 12-well plates for 30 minutes followed by addition of 150
587 mg/l cordycepin (3'-deoxyadenosine, Sigma Aldrich). Immediately after cordycepin
588 addition, samples were vacuum infiltrated for (5 min x 2 times). 15 seedlings for each of
589 samples in triplicates were collected at 0, 15, 30, 60, 120 minutes after cordycepin
590 treatment. Subsequently, total RNA extraction and strand-specific RT-qPCR analyses
591 were carried out by using cDNA as a template synthesized with SuperScript IV Reverse
592 Transcriptase (Invitrogen™) and gene specific primers. *EUKARYOTIC TRANSLATION*

593 *INITIATION FACTOR4A1 (EIF4A1, AT3G13920)* (Perea-Resa et al., 2012) was used as
594 an internal assay control. C_q values at 15, 30, 60, 120 minutes were normalized with C_q
595 at 0 minute and RNA degradation curve obtained following $[C_q(n) = (\ln(C_q/C_q(0)) * (-10))]$
596 equation. Finally, $t_{1/2}$ of transcripts was calculated from obtained slope $[t_{1/2} = (\ln_2)/\text{slope}]$.
597 Oligos used can be found in Supplemental Data Set S6.

598

599 **Genome-wide analyses**

600 Detailed bioinformatic methods can be accessed at
601 https://github.com/peterkindgengroup/Meena_et_al_2024. Briefly, a control set of
602 genes without PAS was curated from all expressed genes (22°C RNA-seq data from
603 this study). In order to better define the gene coordinates of both controls and PAS-host
604 genes, we used available TSS-seq data (S4 Table from cited paper) (Nielsen et al.,
605 2019) in combination with the TTS from TAIR10. Gene length was calculated from these
606 curated genomic features. RNAPII datasets were retrieved (GSE95301 at Gene
607 Expression Omnibus) (Liu et al., 2018). Bedgraphs from samples GSM2522253 for
608 PolII_WT were converted to bigwig (Kent et al., 2010). Deeptools (Ramírez et al., 2016)
609 was used to compute ChIP-seq score matrices and to generate metaplots along the
610 gene body. Differentially expressed genes from plaNET-seq were extracted from Table
611 S2 from (Kindgren et al., 2019). To build the plaNET-seq metaplots, the raw sequences
612 (SRR9117170-SRR9117181) were downloaded and processed as indicated in the
613 previously mentioned GitHub repository. Shortly, after the quality control of raw reads,
614 bam files were generated by aligning the sequence reads against the Arabidopsis
615 genome using STAR 2.7.10a (Dobin et al., 2012) and used on ngs.plot (Shen et al.,
616 2014) to generate the meta gene profiles using the in-built TAIR10 genome and the
617 gene lists of interest. A few existing datasets were remapped for this study. They
618 include DR-seq (Schurch et al., 2014), CAGE (Thieffry et al., 2020), and plaNET-seq
619 (Kindgren et al., 2019).

620

621 **DATA AVAILABILITY**

622 RNA Seq data for wild type is available online at NCBI under accession number
623 GSE252832. All new code is available at
624 https://github.com/peterkindgrengroup/Meena_et_al_2024. Statistical data are provided
625 in Supplementary Data Set S7.

626

627 **ACCESSION NUMBERS**

628 Arabidopsis Genome Initiative locus identifiers for the genes mentioned in this article
629 are as follows: At1g18710 for *MYB47*, At1g73870 for *COL7*, At2g28200 for *ZAT5*,
630 At5g52510 for *SCL8*, and At4g27310 for *BBX28*.

631

632 **SUPPLEMENTARY DATA**

633 **Supplementary Figure S1.** Half-life and RNAPII occupancy of PAS genes.

634 **Supplementary Figure S2.** PAS transcription in response to cold temperature.

635 **Supplementary Figure S3.** RNA level of *ZAT5* and *BBX28* with control at different ZT
636 and freezing test of non-acclimated *zat5-1* and *bbx28-1* plants.

637 **Supplementary Figure S4.** LUCIFERASE assay for *ZAT5* constructs.

638 **Supplementary Figure S5.** RNA stability of *ZAT5* and *BBX28* in CRISPR mutants.

639 **Supplementary Data Set S1.** List of PAS genes.

640 **Supplementary Data Set S2.** Full list of GO terms.

641 **Supplementary Data Set S3.** Differentially expressed genes in the RNA-seq
642 experiment.

643 **Supplementary Data Set S4.** Differentially expressed PAS genes.

644 **Supplementary Data Set S5.** PAS genes with similar expression profile to *CBF2*.

645 **Supplementary Data Set S6.** Oligos used in this study.

646 **Supplementary Data Set S7.** Statistical data.

647

648 **FUNDING INFORMATION**

649 This research was funded by the Swedish research council (2018-03926), FORMAS
650 (2021-01065), Carl Trygger foundation (20:224), and grants from the Knut and Alice
651 Wallenberg Foundation and the Swedish Governmental Agency for Innovation Systems
652 [KAW 2016.0355 and 2020.0240, VINNOVA 2016-00504].

653

654 **ACKNOWLEDGMENTS**

655 We would like to thank members of the Kindgren lab for their critical reading of the
656 manuscript. A special thanks to Linda Allo, Julia Viklander and Tim te Morsche for
657 assistance with the CRISPR-Cas9 constructs. We would like to thank the greenhouse
658 personnel at Umeå Plant Science Centre for plant maintenance and Nicolas Delhomme
659 for bioinformatic help.

660

661 **AUTHOR CONTRIBUTIONS**

662 designed the research (SKM, SSB, VZ, PK); performed research (SKM, CV, SSB, VZ,
663 PK); analyzed data (SKM, MQ, CV, SSB, VZ, SMN, PK); wrote the paper (SKM, MQ,
664 CV, SSB, VZ, SMN, PK).

665

666 **FIGURE LEGENDS**

667 **Figure 1. Poly(A) antisense (PAS) genes are overrepresented by stress-**
668 **responsive transcription factors.**

669 **A)** Graphical representation of the definition of PAS genes. Abbreviations: TSS:
670 transcription start site, AS: antisense.

671 **B)** GO term enrichment of PAS genes (molecular function). The number in bars
672 indicates found number of genes/expected number of genes.

673 **C)** GO term enrichment of PAS genes (biological processes). The number in bars
674 indicates found number of genes/expected number of found genes.

675 **D)** Example of a PAS gene (*WRKY48*, At5g49520). Screenshots showing plaNET-seq
676 expression profile from datasets at 22° C, 3 hours, and 12 hours post cold treatment.
677 Elevated transcriptional activity indicated by higher peaks density and amplitude.

678

679 **Figure 2. PAS genes are highly expressed, but their mRNA is degraded rapidly.**

680 **A)** Violin plot of the length of PAS non-TF genes, TFs non-PAS, PAS TF genes and all
681 expressed genes. Center line, median; box limits, upper and lower quartiles; whiskers,
682 1.5x interquartile range. *p* value was calculated with Mann-Whitney U test and $p < 0.05$
683 was considered significant.

684 **B)** Violin plot of the steady-state level of PAS non-TF genes, TFs non-PAS, PAS TF
685 genes and all expressed genes. Center line, median; box limits, upper and lower
686 quartiles; whiskers, 1.5x interquartile range. *p* value was calculated with Mann-Whitney
687 U test and $p < 0.05$ was considered significant.

688 **C)** Violin plot of the decay rate of PAS non-TF genes, TFs non-PAS, PAS TF genes and
689 all expressed genes after transcriptional inhibition by cordycepin. Center line, median;
690 box limits, upper and lower quartiles; whiskers, 1.5x interquartile range. *p* value was
691 calculated with Mann-Whitney U test and $p < 0.05$ was considered significant.

692 **D)** Metagene analysis of plaNET-seq data of PAS non-TF genes (light blue), TFs non-
693 PAS (grey), PAS TF genes (blue) and all expressed genes (black). The shaded area
694 shows a 95% confidence interval for the mean.

695

696 **Figure 3. Discrepancy between plaNET-seq and RNA-seq.**

697 **A)** Number of total genes differentially expressed in RNA-seq and plaNET-seq after 3
698 and 12 hours of 4°C exposure. The overlap between the two sequencing techniques is
699 shown in darker grey.

700 **B-C)** Correlation plots between differentially expressed genes in RNA-seq and plaNET-
701 seq (UP: grey squares, DOWN: grey diamonds) after **B)** 3 hours of 4°C and **C)** 12 hours
702 of 4°C. The genes plotted come from the overlap seen in **A)**.

703 **D)** Number of PAS genes differentially expressed in RNA-seq and plaNET-seq after 3
704 and 12 hours of 4°C exposure. The overlap between the two sequencing techniques is
705 shown in blue.

706 **E-F)** Correlation plots between differentially expressed PAS genes in RNA-seq and
707 plaNET-seq (UP: blue squares, DOWN: blue diamonds) after **E)** 3 hours of 4°C and **F)**
708 12 hours of 4°C. The genes plotted come from the overlap seen in **D)**.

709

710 **Figure 4. PAS genes have enhanced cold responsiveness.**

711 **A)** Metagene analysis of the plaNET-seq signal (at 22°C) in a 500 bp window centered
712 at the +1 nucleosome. PAS genes that will be UP after 3h at 4°C are shown in blue,
713 genes without antisense transcription but UP after 3h at 4°C are shown grey, and non-
714 DE genes are shown in black. The shaded area shows a 95% confidence interval for
715 the mean.

716 **B)** Metagene analysis of plaNET-seq data (at 22°C). PAS genes that will be UP after 3h
717 at 4°C are shown in blue, genes without antisense transcription but UP after 3h at 4°C
718 are shown in grey, and non-DE genes are shown in black. The shaded area shows a
719 95% confidence interval for the mean.

720 **C)** Metagene analysis of the plaNET-seq signal (after 3h at 4°C) in a 500 bp window
721 centered at the +1 nucleosome. PAS UP genes after 3h at 4°C are shown in blue,
722 genes without antisense transcription but UP after 3h at 4°C are shown in grey, and
723 non-DE genes are shown in black. The shaded area shows a 95% confidence interval
724 for the mean.

725 **D)** Metagene analysis of plaNET-seq data (after 3h at 4°C). PAS UP genes after 3h at
726 4°C are shown in blue, genes without antisense transcription but UP after 3h at 4°C are

727 shown in grey, and non-DE genes are shown in black. The shaded area shows a 95%
728 confidence interval for the mean.

729

730 **Figure 5. *ZAT5* and *BBX28* mRNA show decreased stability at 4°C.**

731 **A)** At4g254970 (*CBF2*). Screenshots are from plaNET-seq and RNA-seq datasets.
732 Elevated transcriptional activity indicated by higher peaks density and amplitude.

733 **B)** At3g17609 (*HYH*). Screenshots are from plaNET-seq and RNA-seq datasets.
734 Elevated transcriptional activity indicated by higher peaks density and amplitude.

735 **C-H)** Transcript stability assays for **C)** *EIF4A1*, **D)** *ZAT5*, **E)** *BBX28*, **F)** *COL7* **G)**
736 *MYB47*, and **H)** *SCL8* after transcriptional inhibition with cordycepin at 22°C and 4°C.
737 Half-life ($t_{1/2}$) was determined from the slope of degradation curves that were obtained
738 after RT-qPCR analysis of cordycepin treated seedlings at indicated time points. Each
739 data point is the mean of three biological replicates. Error bars represent \pm SD.

740

741 **Figure 6. Examples of cold-responsive PAS genes.**

742 **A)** AT2G28200 (*ZAT5*). Screenshots are from plaNET-seq and RNA-seq datasets.
743 Elevated transcriptional activity indicated by higher peaks density and amplitude.

744 **B)** AT4G27310 (*BBX28*). Screenshots are from plaNET-seq and RNA-seq datasets.
745 Elevated transcriptional activity indicated by higher peaks density and amplitude.

746

747 **Figure 7. *ZAT5* and *BBX28* are important for cold acclimation.**

748 **A)** The relative steady-state level of *ZAT5* measured by RT-qPCR following cold
749 exposure (4°C). Steady-state levels were normalized to WT levels at 22°C. The mean
750 values are from three biological replicates. Error bars represent \pm SEM. Statistical
751 significance was calculated with Student's t-test (* $p < 0.05$).

752 **B)** The relative steady-state level of *BBX28* measured by RT-qPCR following cold
753 exposure (4°C). Steady-state levels were normalized to WT levels at 22°C. The mean
754 values are from three biological replicates. Error bars represent \pm SEM. Statistical
755 significance was calculated with Student's t-test (* $p < 0.05$).

756 **C)** Electrolyte leakage in wild-type and *zat5-1* of cold-acclimated (4 days of 4°C) plants.
757 Each data point represents the mean from at least 3 biological replicates (\pm SEM). The
758 dashed line represents the threshold value, 50%. The dotted lines represent the curve
759 fit. Statistical significance was calculated with an extra sum-of-squares F test and the p
760 value is shown in the figure.

761 **D)** Electrolyte leakage in wild-type and *bbx28-1* of cold-acclimated (4 days of 4°C)
762 plants. Each data point represents the mean from at least 3 biological replicates
763 (\pm SEM). The dashed line represents the threshold value, 50%. The dotted lines
764 represent the curve fit. Statistical significance was calculated with an extra sum-of-
765 squares F test and the p value is shown in the figure.

766

767 **Figure 8. Characterization of *asZAT5* and *asBBX28*.**

768 Screenshots from plaNET-seq (upper panel), CAGE (middle panel), and DRS-seq
769 (lower panel) for **A)** *ZAT5*, and **B)** *BBX28*. 0 indicates the TSS of the sense transcript.
770 Elevated transcriptional activity indicated by higher peaks density and amplitude.

771

772 **Figure 9. *asZAT5* and *asBBX28* are important for proper regulation of their host** 773 **gene.**

774 **A)** Graphical representation of the *ZAT5* and the *BBX28* loci showing the location of
775 sequence targeted by CRISPR-Cas9 to generate an *asZAT5* knockdown line (*aszat5-1*)
776 and an *asBBX28* knockdown line (*asbbx28-1*). Antisense transcription start site (*asTSS*)
777 window and distances of knocked out genomic sequence from 3'-end are marked with
778 dotted lines. Location of RT-qPCR probes for sense and antisense are shown.

779 **B)** The relative nascent and steady-state level of *asZAT5* and *ZAT5* in wild-type and
780 *aszat5-1* measured by RT-qPCR at 22°C and following 3h of cold exposure (4°C). All
781 levels were normalized to WT levels at 22°C. The mean values are from three biological
782 replicates. Error bars represent \pm SEM. Statistical significance was calculated with
783 Student's t-test (* $p < 0.05$).

784 **C)** Electrolyte leakage in wild-type and *aszat5-1* of cold-acclimated (5 days of 4°C)
785 plants. Each data point represents the mean from at least 3 biological replicates
786 (\pm SEM). The dashed line represents the threshold value, 50%. The dotted lines
787 represent the curve fit. Statistical significance was calculated with an extra sum-of-
788 squares F test and the p value is shown in the figure.

789 **D)** The relative steady-state level of *asBBX28* and *BBX28* in wild-type and *asbbx28-1*
790 measured by RT-qPCR at 22°C and following 3h of cold exposure (4°C). All levels were
791 normalized to WT levels at 22°C. The mean values are from three biological replicates.
792 Error bars represent \pm SEM. Statistical significance was calculated with Student's t-test
793 (* $p < 0.05$).

794 **E)** Electrolyte leakage in wild-type and *asbbx28-1* of cold-acclimated (5 days of 4°C)
795 plants. Each data point represents the mean from at least 3 biological replicates
796 (\pm SEM). The dashed line represents the threshold value, 50%. The dotted lines
797 represent the curve fit. Statistical significance was calculated with an extra sum-of-
798 squares F test and the p value is shown in the figure.

799

800 REFERENCES

801 Archacki, R., Yatusевич, R., Buszewicz, D., Krzyczmonik, K., Patryn, J., Iwanicka-
802 Nowicka, R., Biecek, P., Wilczynski, B., Koblowska, M., Jerzmanowski, A.,
803 and Swiezewski, S. (2017). Arabidopsis SWI/SNF chromatin remodeling
804 complex binds both promoters and terminators to regulate gene expression.
805 Nucleic Acids Res **45**, 3116-3129.

806 Ariel, F., Jegu, T., Latrasse, D., Romero-Barrios, N., Christ, A., Benhamed, M., and
807 Crespi, M. (2014). Noncoding Transcription by Alternative RNA Polymerases

808 Dynamically Regulates an Auxin-Driven Chromatin Loop. *Molecular Cell* **55**, 383-
809 396.

810 **Ariel, F., Lucero, L., Christ, A., Mammarella, M.F., Jegu, T., Veluchamy, A.,**
811 **Mariappan, K., Latrasse, D., Blein, T., Liu, C., Benhamed, M., and Crespi, M.**
812 (2020). R-Loop Mediated trans Action of the APOLO Long Noncoding RNA.
813 *Molecular Cell* **77**, 1055-1065.e1054.

814 **Bolger, A.M., Lohse, M., and Usadel, B.** (2014). Trimmomatic: a flexible trimmer for
815 Illumina sequence data. *Bioinformatics* **30**, 2114-2120.

816 **Borsani, O., Zhu, J., Verslues, P.E., Sunkar, R., and Zhu, J.-K.** (2005). Endogenous
817 siRNAs Derived from a Pair of Natural cis-Antisense Transcripts Regulate Salt
818 Tolerance in Arabidopsis. *Cell* **123**, 1279-1291.

819 **Brown, T., Howe, F.S., Murray, S.C., Wouters, M., Lorenz, P., Seward, E., Rata, S.,**
820 **Angel, A., and Mellor, J.** (2018). Antisense transcription-dependent chromatin
821 signature modulates sense transcript dynamics. *Molecular Systems Biology* **14**,
822 e8007.

823 **Cao, J., Liang, Y., Yan, T., Wang, X., Zhou, H., Chen, C., Zhang, Y., Zhang, B.,**
824 **Zhang, S., Liao, J., Cheng, S., Chu, J., Huang, X., Xu, D., Li, J., Deng, X.W.,**
825 **and Lin, F.** (2022). The photomorphogenic repressors BBX28 and BBX29
826 integrate light and brassinosteroid signaling to inhibit seedling development in
827 Arabidopsis. *Plant Cell* **34**, 2266-2285.

828 **Chen, M.-X., Zhu, F.-Y., Gao, B., Ma, K.-L., Zhang, Y., Fernie, A.R., Chen, X., Dai, L.,**
829 **Ye, N.-H., Zhang, X., Tian, Y., Zhang, D., Xiao, S., Zhang, J., and Liu, Y.-G.**
830 (2019). Full-Length Transcript-Based Proteogenomics of Rice Improves Its
831 Genome and Proteome Annotation1. *Plant Physiology* **182**, 1510-1526.

832 **Chiba, Y., Mineta, K., Hirai, M.Y., Suzuki, Y., Kanaya, S., Takahashi, H., Onouchi,**
833 **H., Yamaguchi, J., and Naito, S.** (2012). Changes in mRNA Stability Associated
834 with Cold Stress in Arabidopsis Cells. *Plant and Cell Physiology* **54**, 180-194.

835 **Csorba, T., Questa, J.I., Sun, Q., and Dean, C.** (2014). Antisense *COOLAIR* mediates
836 the coordinated switching of chromatin states at *FLC* during vernalization.
837 *Proceedings of the National Academy of Sciences* **111**, 16160-16165.

838 **Delhomme, N., Zare, A., Shutava, I., Kochakarn, T.F., Mähler, N., Serrano, A., Irani-**
839 **Shemirani, M., and Evanzalen.** (2023). UPSCb/UPSCb-common: Release as of
840 15th December 2023 (Version v20231215). Zenodo.

841 **Ding, Y., Virlouvét, L., Liu, N., Riethoven, J.-J., Fromm, M., and Avramova, Z.**
842 (2014). Dehydration stress memory genes of *Zea mays*; comparison with
843 *Arabidopsis thaliana*. *BMC Plant Biology* **14**, 141.

844 **Dobin, A., Davis, C.A., Schlesinger, F., Drenkow, J., Zaleski, C., Jha, S., Batut, P.,**
845 **Chaisson, M., and Gingeras, T.R.** (2012). STAR: ultrafast universal RNA-seq
846 aligner. *Bioinformatics* **29**, 15-21.

847 **Fedak, H., Palusinska, M., Krzyczmonik, K., Brzezniak, L., Yatusевич, R., Pietras,**
848 **Z., Kaczanowski, S., and Swiezewski, S.** (2016). Control of seed dormancy in
849 *Arabidopsis* by a cis-acting noncoding antisense transcript. *Proceedings of the*
850 *National Academy of Sciences* **113**, E7846-E7855.

851 **Held, M.A., Penning, B., Brandt, A.S., Kessans, S.A., Yong, W., Scofield, S.R., and**
852 **Carpita, N.C.** (2008). Small-interfering RNAs from natural antisense transcripts
853 derived from a cellulose synthase gene modulate cell wall biosynthesis in barley.
854 *Proceedings of the National Academy of Sciences* **105**, 20534-20539.

855 **Henriques, R., Wang, H., Liu, J., Boix, M., Huang, L.F., and Chua, N.H.** (2017). The
856 antiphasic regulatory module comprising CDF5 and its antisense RNA FLORE
857 links the circadian clock to photoperiodic flowering. *New Phytol* **216**, 854-867.

858 **Henz, S.R., Cumbie, J.S., Kasschau, K.D., Lohmann, J.U., Carrington, J.C., Weigel,**
859 **D., and Schmid, M.** (2007). Distinct Expression Patterns of Natural Antisense
860 Transcripts in *Arabidopsis*. *Plant Physiology* **144**, 1247-1255.

861 **Jabnoune, M., Secco, D., Lecampion, C., Robaglia, C., Shu, Q., and Poirier, Y.**
862 (2013). A rice cis-natural antisense RNA acts as a translational enhancer for its
863 cognate mRNA and contributes to phosphate homeostasis and plant fitness.
864 *Plant Cell* **25**, 4166-4182.

865 **Katiyar-Agarwal, S., Morgan, R., Dahlbeck, D., Borsani, O., Villegas, A., Zhu, J.-K.,**
866 **Staskawicz, B.J., and Jin, H.** (2006). A pathogen-inducible endogenous siRNA
867 in plant immunity. *Proceedings of the National Academy of Sciences* **103**, 18002-
868 18007.

- 869 **Kent, W.J., Zweig, A.S., Barber, G., Hinrichs, A.S., and Karolchik, D.** (2010). BigWig
870 and BigBed: enabling browsing of large distributed datasets. *Bioinformatics* **26**,
871 2204-2207.
- 872 **Kindgren, P., Dubreuil, C., and Strand, Å.** (2015). The Recovery of Plastid Function Is
873 Required for Optimal Response to Low Temperatures in Arabidopsis. *PLOS ONE*
874 **10**, e0138010.
- 875 **Kindgren, P., Ivanov, M., and Marquardt, S.** (2019). Native elongation transcript
876 sequencing reveals temperature dependent dynamics of nascent RNAPII
877 transcription in Arabidopsis. *Nucleic Acids Research* **48**, 2332-2347.
- 878 **Kindgren, P., Ard, R., Ivanov, M., and Marquardt, S.** (2018). Transcriptional read-
879 through of the long non-coding RNA SVALKA governs plant cold acclimation.
880 *Nature Communications* **9**, 4561.
- 881 **Kopylova, E., Noé, L., and Touzet, H.** (2012). SortMeRNA: fast and accurate filtering
882 of ribosomal RNAs in metatranscriptomic data. *Bioinformatics* **28**, 3211-3217.
- 883 **Lampropoulos, A., Sutikovic, Z., Wenzl, C., Maegele, I., Lohmann, J.U., and
884 Forner, J.** (2013). GreenGate---a novel, versatile, and efficient cloning system
885 for plant transgenesis. *PLoS One* **8**, e83043.
- 886 **Lange, H., Zuber, H., Sement, F.M., Chicher, J., Kuhn, L., Hammann, P., Brunaud,
887 V., Bérard, C., Bouteiller, N., Balzergue, S., Aubourg, S., Martin-Magniette,
888 M.-L., Vaucheret, H., and Gagliardi, D.** (2014). The RNA Helicases AtMTR4
889 and HEN2 Target Specific Subsets of Nuclear Transcripts for Degradation by the
890 Nuclear Exosome in Arabidopsis thaliana. *PLOS Genetics* **10**, e1004564.
- 891 **Li, C., Gu, L., Gao, L., Chen, C., Wei, C.-Q., Qiu, Q., Chien, C.-W., Wang, S., Jiang,
892 L., Ai, L.-F., Chen, C.-Y., Yang, S., Nguyen, V., Qi, Y., Snyder, M.P.,
893 Burlingame, A.L., Kohalmi, S.E., Huang, S., Cao, X., Wang, Z.-Y., Wu, K.,
894 Chen, X., and Cui, Y.** (2016). Concerted genomic targeting of H3K27
895 demethylase REF6 and chromatin-remodeling ATPase BRM in Arabidopsis.
896 *Nature Genetics* **48**, 687-693.
- 897 **Li, X., Yang, Q., Liao, X., Tian, Y., Zhang, F., Zhang, L., and Liu, Q.** (2022). A natural
898 antisense RNA improves chrysanthemum cold tolerance by regulating the
899 transcription factor DgTCP1. *Plant Physiology*.

- 900 **Liu, C., Xin, Y., Xu, L., Cai, Z., Xue, Y., Liu, Y., Xie, D., Liu, Y., and Qi, Y.** (2018).
901 Arabidopsis ARGONAUTE 1 Binds Chromatin to Promote Gene Transcription in
902 Response to Hormones and Stresses. *Developmental Cell* **44**, 348-361.e347.
- 903 **Liu, M., Zhu, J., and Dong, Z.** (2021). Immediate transcriptional responses of
904 Arabidopsis leaves to heat shock. *Journal of Integrative Plant Biology* **63**, 468-
905 483.
- 906 **Love, M.I., Huber, W., and Anders, S.** (2014). Moderated estimation of fold change
907 and dispersion for RNA-seq data with DESeq2. *Genome Biology* **15**, 550.
- 908 **Lucero, L., Ferrero, L., Fonouni-Farde, C., and Ariel, F.** (2021). Functional
909 classification of plant long noncoding RNAs: a transcript is known by the
910 company it keeps. *New Phytologist* **229**, 1251-1260.
- 911 **Mao, Y.S., Sunwoo, H., Zhang, B., and Spector, D.L.** (2011). Direct visualization of
912 the co-transcriptional assembly of a nuclear body by noncoding RNAs. *Nature*
913 *Cell Biology* **13**, 95-101.
- 914 **Marquis, V., Smirnova, E., Graindorge, S., Delcros, P., Villette, C., Zumsteg, J.,**
915 **Heintz, D., and Heitz, T.** (2022). Broad-spectrum stress tolerance conferred by
916 suppressing jasmonate signaling attenuation in Arabidopsis JASMONIC ACID
917 OXIDASE mutants. *The Plant Journal* **109**, 856-872.
- 918 **Matsui, A., Ishida, J., Morosawa, T., Mochizuki, Y., Kaminuma, E., Endo, T.A.,**
919 **Okamoto, M., Nambara, E., Nakajima, M., Kawashima, M., Satou, M., Kim, J.-**
920 **M., Kobayashi, N., Toyoda, T., Shinozaki, K., and Seki, M.** (2008). Arabidopsis
921 Transcriptome Analysis under Drought, Cold, High-Salinity and ABA Treatment
922 Conditions using a Tiling Array. *Plant and Cell Physiology* **49**, 1135-1149.
- 923 **Mayer, A., di Iulio, J., Maleri, S., Eser, U., Vierstra, J., Reynolds, A., Sandstrom, R.,**
924 **Stamatoyannopoulos, John A., and Churchman, L.S.** (2015). Native
925 Elongating Transcript Sequencing Reveals Human Transcriptional Activity at
926 Nucleotide Resolution. *Cell* **161**, 541-554.
- 927 **Murray, S.C., Haenni, S., Howe, F.S., Fischl, H., Chocian, K., Nair, A., and Mellor, J.**
928 (2015). Sense and antisense transcription are associated with distinct chromatin
929 architectures across genes. *Nucleic Acids Research* **43**, 7823-7837.

- 930 **Narsai, R., Howell, K.A., Millar, A.H., O'Toole, N., Small, I., and Whelan, J. (2007).**
931 Genome-Wide Analysis of mRNA Decay Rates and Their Determinants in
932 *Arabidopsis thaliana*. *Plant Cell* **19**, 3418-3436.
- 933 **Nielsen, M., Ard, R., Leng, X., Ivanov, M., Kindgren, P., Pelechano, V., and**
934 **Marquardt, S. (2019).** Transcription-driven chromatin repression of Intragenic
935 transcription start sites. *PLOS Genetics* **15**, e1007969.
- 936 **Parent, J.-S., Jauvion, V., Bouché, N., Béclin, C., Hachet, M., Zytnicki, M., and**
937 **Vaucheret, H. (2015).** Post-transcriptional gene silencing triggered by sense
938 transgenes involves uncapped antisense RNA and differs from silencing
939 intentionally triggered by antisense transgenes. *Nucleic Acids Research* **43**,
940 8464-8475.
- 941 **Patro, R., Duggal, G., Love, M.I., Irizarry, R.A., and Kingsford, C. (2017).** Salmon
942 provides fast and bias-aware quantification of transcript expression. *Nature*
943 *Methods* **14**, 417-419.
- 944 **Perea-Resa, C., Hernández-Verdeja, T., López-Cobollo, R., Castellano, M.d.M., and**
945 **Salinas, J. (2012).** LSM Proteins Provide Accurate Splicing and Decay of
946 Selected Transcripts to Ensure Normal *Arabidopsis* Development. *Plant Cell* **24**,
947 4930-4947.
- 948 **Ramírez, F., Ryan, D.P., Grüning, B., Bhardwaj, V., Kilpert, F., Richter, A.S., Heyne,**
949 **S., Dündar, F., and Manke, T. (2016).** deepTools2: a next generation web
950 server for deep-sequencing data analysis. *Nucleic Acids Research* **44**, W160-
951 W165.
- 952 **Reis, R.S., and Poirier, Y. (2021).** Making sense of the natural antisense transcript
953 puzzle. *Trends in Plant Science* **26**, 1104-1115.
- 954 **Romanowski, A., Schlaen, R.G., Perez-Santangelo, S., Mancini, E., and Yanovsky,**
955 **M.J. (2020).** Global transcriptome analysis reveals circadian control of splicing
956 events in *Arabidopsis thaliana*. *The Plant Journal* **103**, 889-902.
- 957 **Roulé, T., Christ, A., Hussain, N., Huang, Y., Hartmann, C., Benhamed, M.,**
958 **Gutierrez-Marcos, J., Ariel, F., Crespi, M., and Blein, T. (2022).** The lncRNA
959 MARS modulates the epigenetic reprogramming of the marneral cluster in
960 response to ABA. *Molecular Plant* **15**, 840-856.

- 961 **Schurch, N.J., Cole, C., Sherstnev, A., Song, J., Duc, C., Storey, K.G., McLean,**
962 **W.H.I., Brown, S.J., Simpson, G.G., and Barton, G.J.** (2014). Improved
963 Annotation of 3' Untranslated Regions and Complex Loci by Combination of
964 Strand-Specific Direct RNA Sequencing, RNA-Seq and ESTs. *PLOS ONE* **9**,
965 e94270.
- 966 **Shen, L., Shao, N., Liu, X., and Nestler, E.** (2014). ngs.plot: Quick mining and
967 visualization of next-generation sequencing data by integrating genomic
968 databases. *BMC Genomics* **15**, 284.
- 969 **Sidaway-Lee, K., Costa, M.J., Rand, D.A., Finkenstadt, B., and Penfield, S.** (2014).
970 Direct measurement of transcription rates reveals multiple mechanisms for
971 configuration of the Arabidopsis ambient temperature response. *Genome Biology*
972 **15**, R45.
- 973 **Song, Z., Yan, T., Liu, J., Bian, Y., Heng, Y., Lin, F., Jiang, Y., Wang Deng, X., and**
974 **Xu, D.** (2020). BBX28/BBX29, HY5 and BBX30/31 form a feedback loop to fine-
975 tune photomorphogenic development. *The Plant Journal* **104**, 377-390.
- 976 **Sorenson, R.S., Deshotel, M.J., Johnson, K., Adler, F.R., and Sieburth, L.E.** (2018).
977 Arabidopsis mRNA decay landscape arises from specialized RNA decay
978 substrates, decapping-mediated feedback, and redundancy. *Proceedings of the*
979 *National Academy of Sciences* **115**, E1485-E1494.
- 980 **Swiezewski, S., Liu, F., Magusin, A., and Dean, C.** (2009). Cold-induced silencing by
981 long antisense transcripts of an Arabidopsis Polycomb target. *Nature* **462**, 799-
982 802.
- 983 **Swiezewski, S., Crevillen, P., Liu, F., Ecker, J.R., Jerzmanowski, A., and Dean, C.**
984 (2007). Small RNA-mediated chromatin silencing directed to the 3' region of the
985 Arabidopsis gene encoding the developmental regulator, FLC. *Proceedings of*
986 *the National Academy of Sciences* **104**, 3633-3638.
- 987 **Thieffry, A., Vigh, M.L., Bornholdt, J., Ivanov, M., Brodersen, P., and Sandelin, A.**
988 (2020). Characterization of Arabidopsis thaliana Promoter Bidirectionality and
989 Antisense RNAs by Inactivation of Nuclear RNA Decay Pathways. *Plant Cell* **32**,
990 1845-1867.

- 991 **Wan, Q., Guan, X., Yang, N., Wu, H., Pan, M., Liu, B., Fang, L., Yang, S., Hu, Y., Ye,**
992 **W., Zhang, H., Ma, P., Chen, J., Wang, Q., Mei, G., Cai, C., Yang, D., Wang,**
993 **J., Guo, W., Zhang, W., Chen, X., and Zhang, T.** (2016). Small interfering RNAs
994 from bidirectional transcripts of GhMML3_A12 regulate cotton fiber development.
995 *New Phytologist* **210**, 1298-1310.
- 996 **Wang, H., Chung, P.J., Liu, J., Jang, I.-C., Kean, M.J., Xu, J., and Chua, N.-H.**
997 (2014). Genome-wide identification of long noncoding natural antisense
998 transcripts and their responses to light in Arabidopsis. *Genome Research* **24**,
999 444-453.
- 1000 **Wang, H., Zhang, Z., Li, H., Zhao, X., Liu, X., Ortiz, M., Lin, C., and Liu, B.** (2013).
1001 CONSTANS-LIKE 7 regulates branching and shade avoidance response in
1002 Arabidopsis. *Journal of Experimental Botany* **64**, 1017-1024.
- 1003 **Wierzbicki, A.T., Blevins, T., and Swiezewski, S.** (2021). Long Noncoding RNAs in
1004 Plants. *Annual Review of Plant Biology* **72**, 245-271.
- 1005 **Wu, H.-W., Deng, S., Xu, H., Mao, H.-Z., Liu, J., Niu, Q.-W., Wang, H., and Chua, N.-**
1006 **H.** (2018). A noncoding RNA transcribed from the AGAMOUS (AG) second intron
1007 binds to CURLY LEAF and represses AG expression in leaves. *New Phytologist*
1008 **219**, 1480-1491.
- 1009 **Xing, D.-H., Lai, Z.-B., Zheng, Z.-Y., Vinod, K.M., Fan, B.-F., and Chen, Z.-X.** (2008).
1010 Stress- and Pathogen-Induced Arabidopsis WRKY48 is a Transcriptional
1011 Activator that Represses Plant Basal Defense. *Molecular Plant* **1**, 459-470.
- 1012 **Xing, H.-L., Dong, L., Wang, Z.-P., Zhang, H.-Y., Han, C.-Y., Liu, B., Wang, X.-C.,**
1013 **and Chen, Q.-J.** (2014). A CRISPR/Cas9 toolkit for multiplex genome editing in
1014 plants. *BMC Plant Biology* **14**, 327.
- 1015 **Zacharaki, V., Meena, S.K., and Kindgren, P.** (2023). The non-coding RNA SVALKKA
1016 locus produces a cis-natural antisense transcript that negatively regulates the
1017 expression of CBF1 and biomass production at normal temperatures. *Plant*
1018 *Communications* **4**, 100551.
- 1019 **Zhao, X., Li, J., Lian, B., Gu, H., Li, Y., and Qi, Y.** (2018). Global identification of
1020 Arabidopsis lncRNAs reveals the regulation of MAF4 by a natural antisense
1021 RNA. *Nature Communications* **9**, 5056.

1022 **Zhu, J., Liu, M., Liu, X., and Dong, Z.** (2018). RNA polymerase II activity revealed by
1023 GRO-seq and pNET-seq in Arabidopsis. *Nature Plants* **4**, 1112-1123.

1024

1025

1026

ACCEPTED MANUSCRIPT

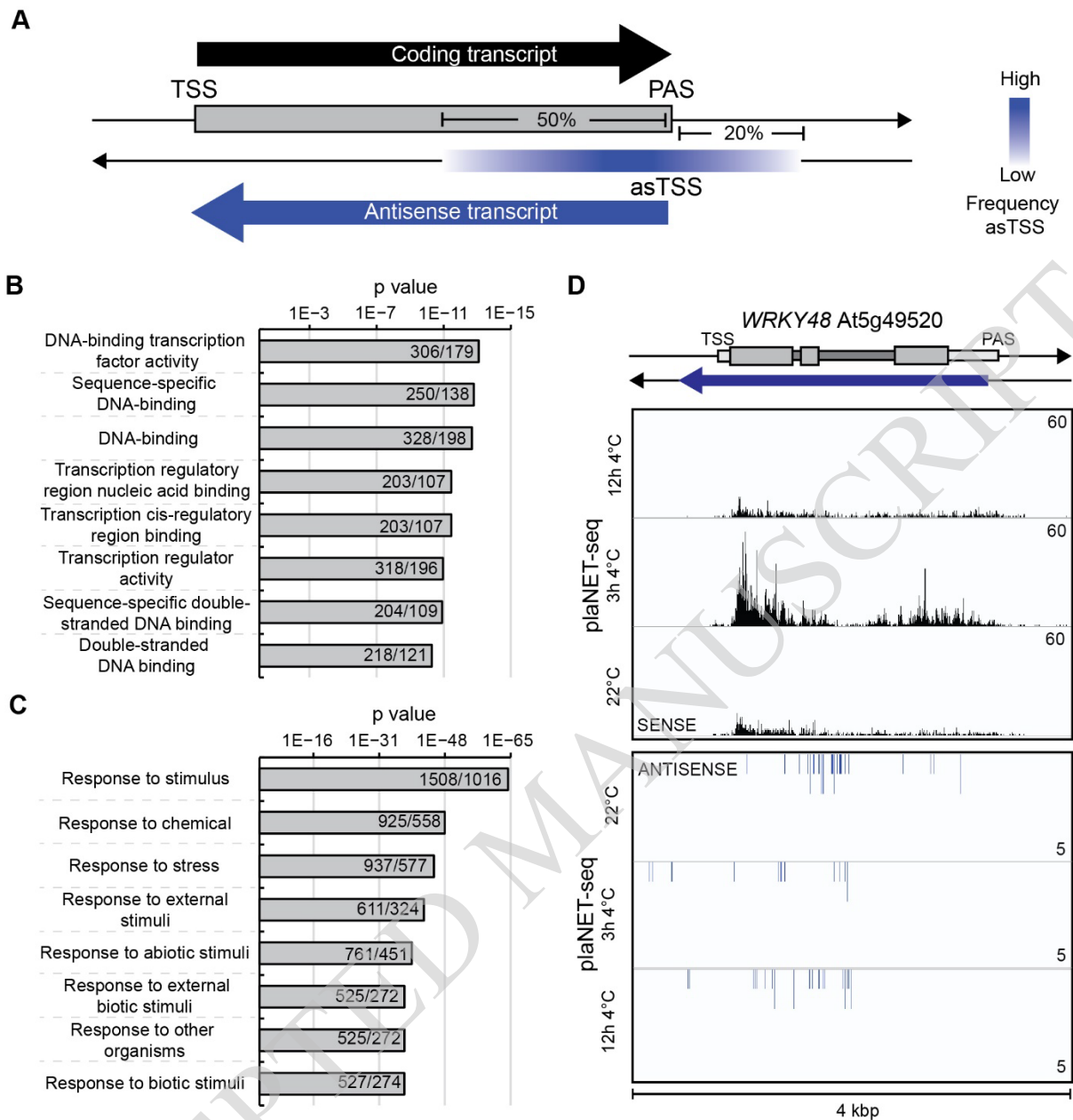


Figure 1. Poly(A) antisense (PAS) genes are overrepresented by stress-responsive transcription factors.

A) Graphical representation of the definition of PAS genes. Abbreviations: TSS: transcription start site, AS: antisense.

B) GO term enrichment of PAS genes (molecular function). The number in bars indicates found number of genes/expected number of genes.

C) GO term enrichment of PAS genes (biological processes). The number in bars indicates found number of genes/expected number of found genes.

D) Example of a PAS gene (*WRKY48*, At5g49520). Screenshots showing plaNET-seq expression profile from datasets at 22° C, 3 hours, and 12 hours post cold treatment. Elevated transcriptional activity indicated by higher peaks density and amplitude.

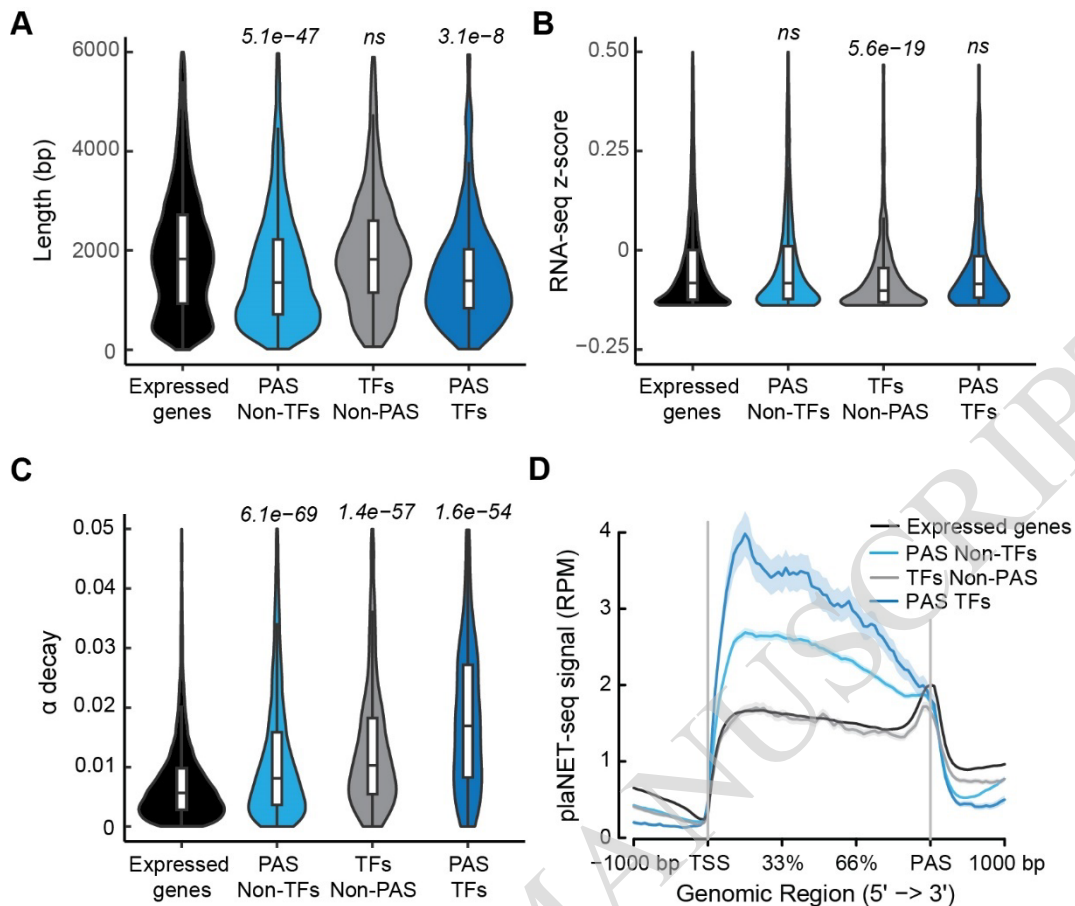


Figure 2. PAS genes are highly expressed, but their mRNA is degraded rapidly.

A) Violin plot of the length of PAS non-TF genes, TFs non-PAS, PAS TF genes and all expressed genes. Center line, median; box limits, upper and lower quartiles; whiskers, 1.5x interquartile range. p value was calculated with Mann-Whitney U test and $p < 0.05$ was considered significant.

B) Violin plot of the steady-state level of PAS non-TF genes, TFs non-PAS, PAS TF genes and all expressed genes. Center line, median; box limits, upper and lower quartiles; whiskers, 1.5x interquartile range. p value was calculated with Mann-Whitney U test and $p < 0.05$ was considered significant.

C) Violin plot of the decay rate of PAS non-TF genes, TFs non-PAS, PAS TF genes and all expressed genes after transcriptional inhibition by cordycepin. Center line, median; box limits, upper and lower quartiles; whiskers, 1.5x interquartile range. p value was calculated with Mann-Whitney U test and $p < 0.05$ was considered significant.

D) Metagene analysis of plaNET-seq data of PAS non-TF genes (light blue), TFs non-PAS (grey), PAS TF genes (blue) and all expressed genes (black). The shaded area shows a 95% confidence interval for the mean.

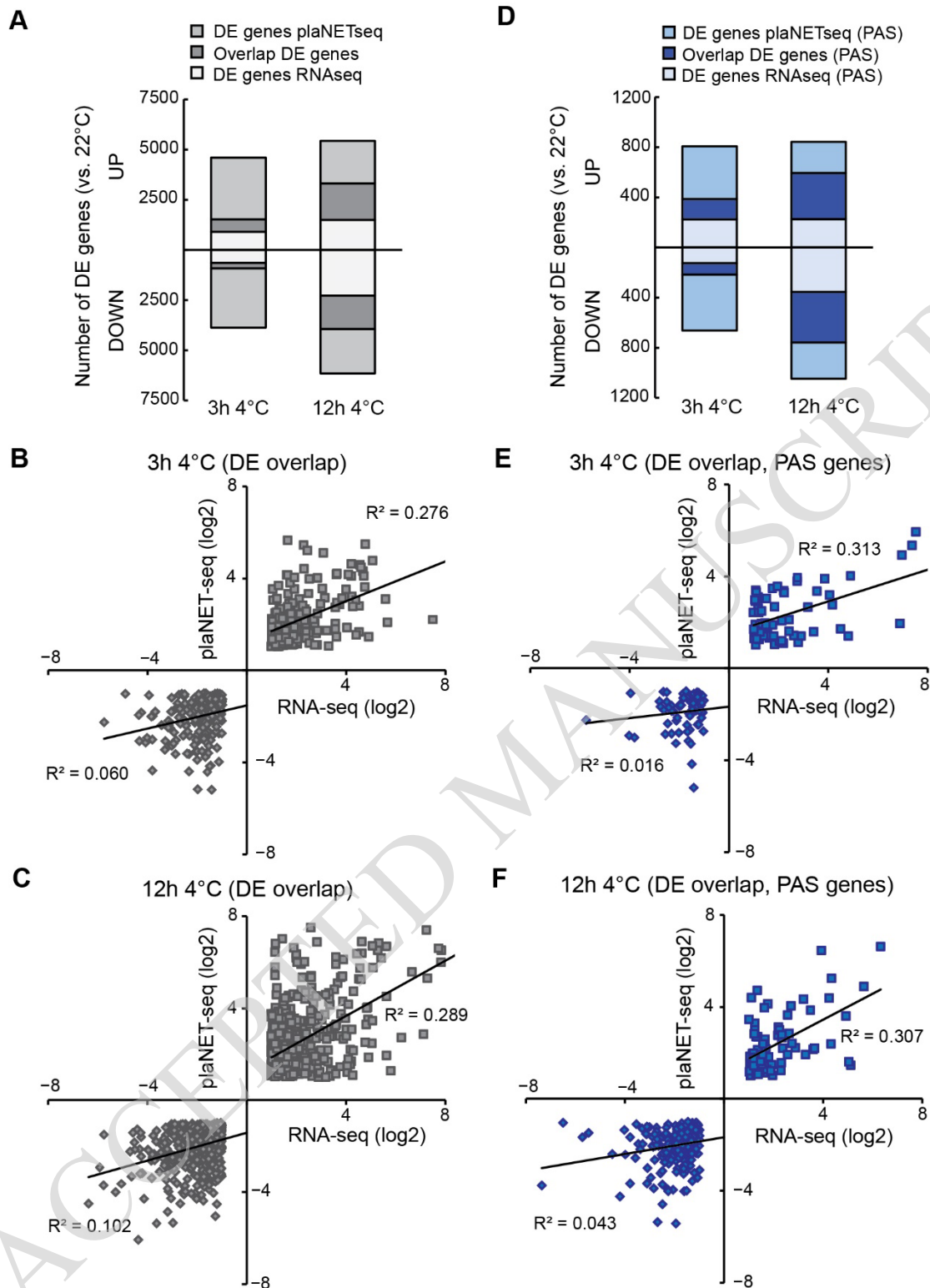


Figure 3. Discrepancy between plaNET-seq and RNA-seq.

A) Number of total genes differentially expressed in RNA-seq and plaNET-seq after 3 and 12 hours of 4°C exposure. The overlap between the two sequencing techniques is shown in darker grey.

B-C) Correlation plots between differentially expressed genes in RNA-seq and plaNET-seq (UP: grey squares, DOWN: grey diamonds) after **B)** 3 hours of 4°C and **C)** 12 hours of 4°C. The genes plotted come from the overlap seen in **A)**.

D) Number of PAS genes differentially expressed in RNA-seq and plaNET-seq after 3 and 12 hours of 4°C exposure. The overlap between the two sequencing techniques is shown in blue.

E-F) Correlation plots between differentially expressed PAS genes in RNA-seq and plaNET-seq (UP: blue squares, DOWN: blue diamonds) after **E)** 3 hours of 4°C and **F)** 12 hours of 4°C. The genes plotted come from the overlap seen in **D)**.

ACCEPTED MANUSCRIPT

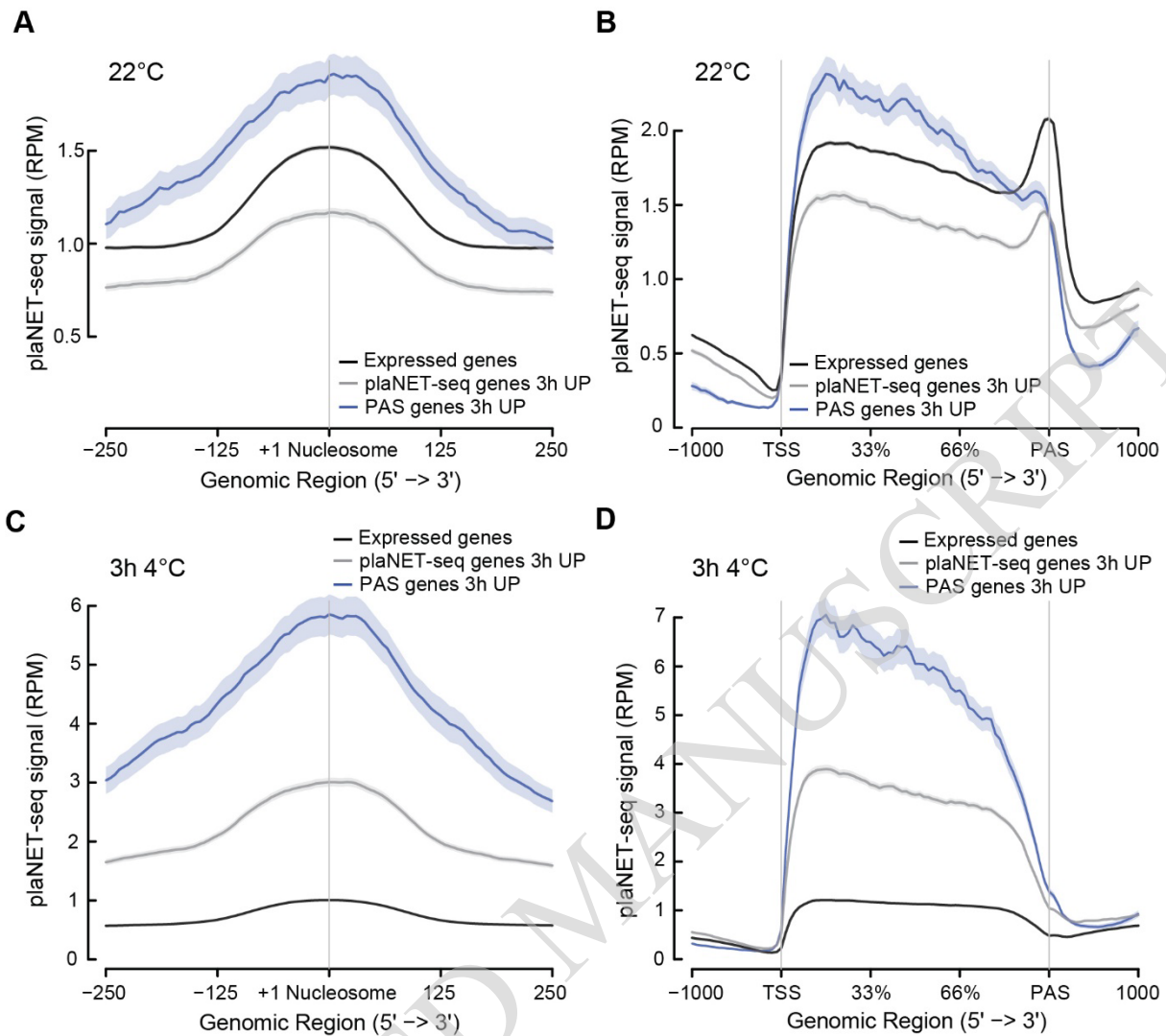


Figure 4. PAS genes have enhanced cold responsiveness.

A) Metagenome analysis of the plaNET-seq signal (at 22°C) in a 500 bp window centered at the +1 nucleosome. PAS genes that will be UP after 3h at 4°C are shown in blue, genes without antisense transcription but UP after 3h at 4°C are shown grey, and non-DE genes are shown in black. The shaded area shows a 95% confidence interval for the mean.

B) Metagenome analysis of plaNET-seq data (at 22°C). PAS genes that will be UP after 3h at 4°C are shown in blue, genes without antisense transcription but UP after 3h at 4°C are shown in grey, and non-DE genes are shown in black. The shaded area shows a 95% confidence interval for the mean.

C) Metagenome analysis of the plaNET-seq signal (after 3h at 4°C) in a 500 bp window centered at the +1 nucleosome. PAS UP genes after 3h at 4°C are shown in blue, genes without antisense transcription but UP after 3h at 4°C are shown in grey, and non-DE genes are shown in black. The shaded area shows a 95% confidence interval for the mean.

D) Metagenome analysis of plaNET-seq data (after 3h at 4°C). PAS UP genes after 3h at 4°C are shown in blue, genes without antisense transcription but UP after 3h at 4°C are shown in grey, and non-DE genes are shown in black. The shaded area shows a 95% confidence interval for the mean.

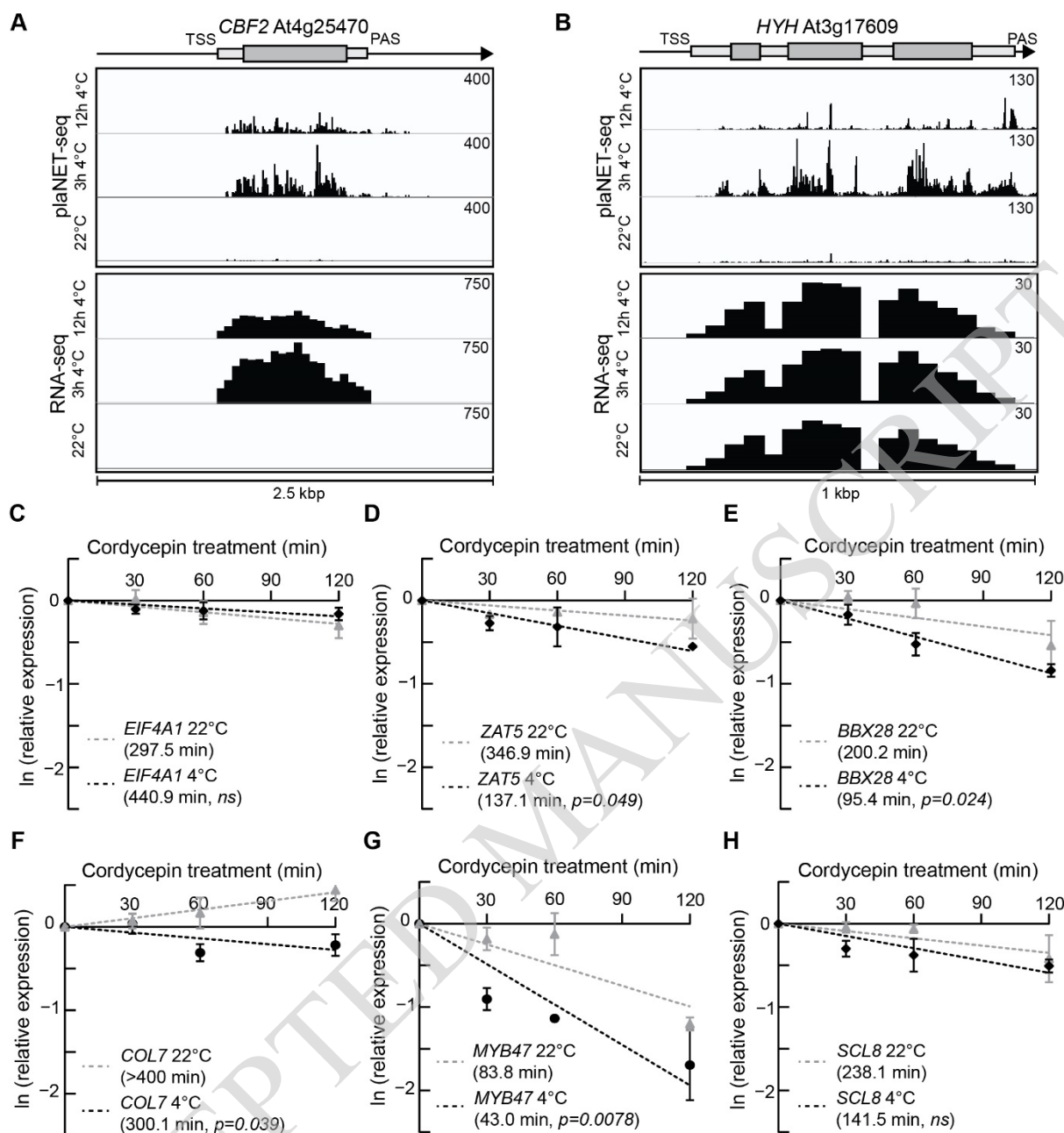


Figure 5. *ZAT5* and *BBX28* mRNA show decreased stability at 4°C.

A) At4g254970 (*CBF2*). Screenshots are from plaNET-seq and RNA-seq datasets. Elevated transcriptional activity indicated by higher peaks density and amplitude.

B) At3g17609 (*HYH*). Screenshots are from plaNET-seq and RNA-seq datasets. Elevated transcriptional activity indicated by higher peaks density and amplitude.

C-H) Transcript stability assays for **C)** *EIF4A1*, **D)** *ZAT5*, **E)** *BBX28*, **F)** *COL7*, **G)** *MYB47*, and **H)** *SCL8* after transcriptional inhibition with cordycepin at 22°C and 4°C. Half-life ($t_{1/2}$) was determined from the slope of degradation curves that were obtained after RT-qPCR analysis of cordycepin treated seedlings at indicated time points. Each data point is the mean of three biological replicates. Error bars represent \pm SD.

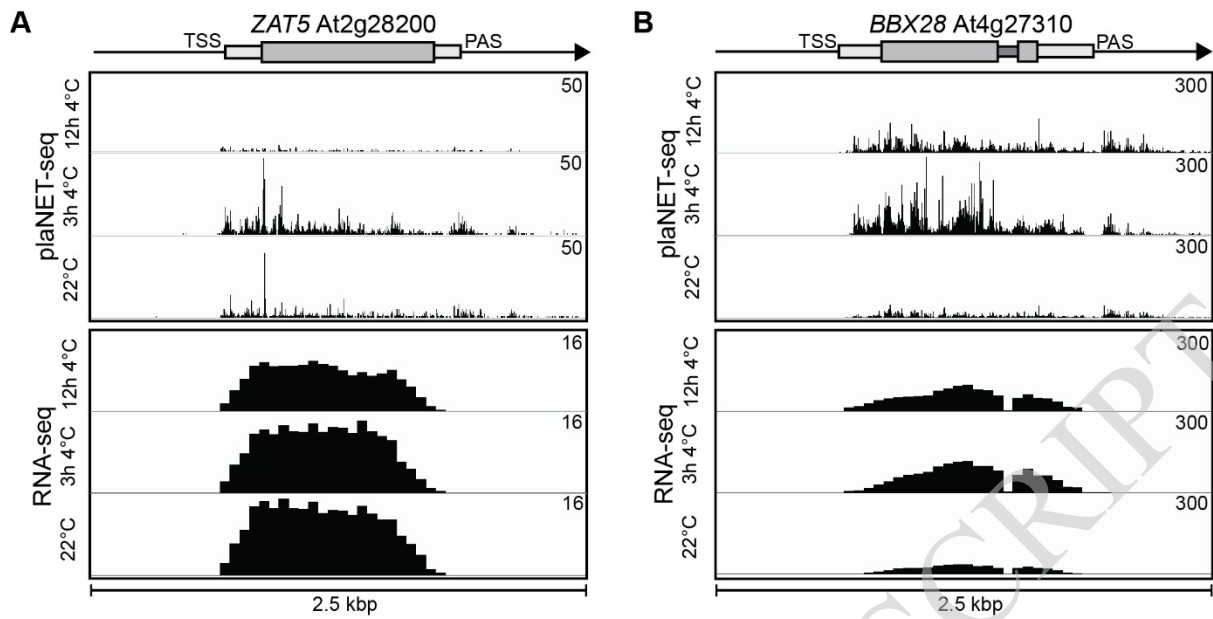


Figure 6. Examples of cold-responsive PAS genes.

A) *AT2G28200* (*ZAT5*). Screenshots are from plaNET-seq and RNA-seq datasets. Elevated transcriptional activity indicated by higher peaks density and amplitude.

B) *AT4G27310* (*BBX28*). Screenshots are from plaNET-seq and RNA-seq datasets. Elevated transcriptional activity indicated by higher peaks density and amplitude.

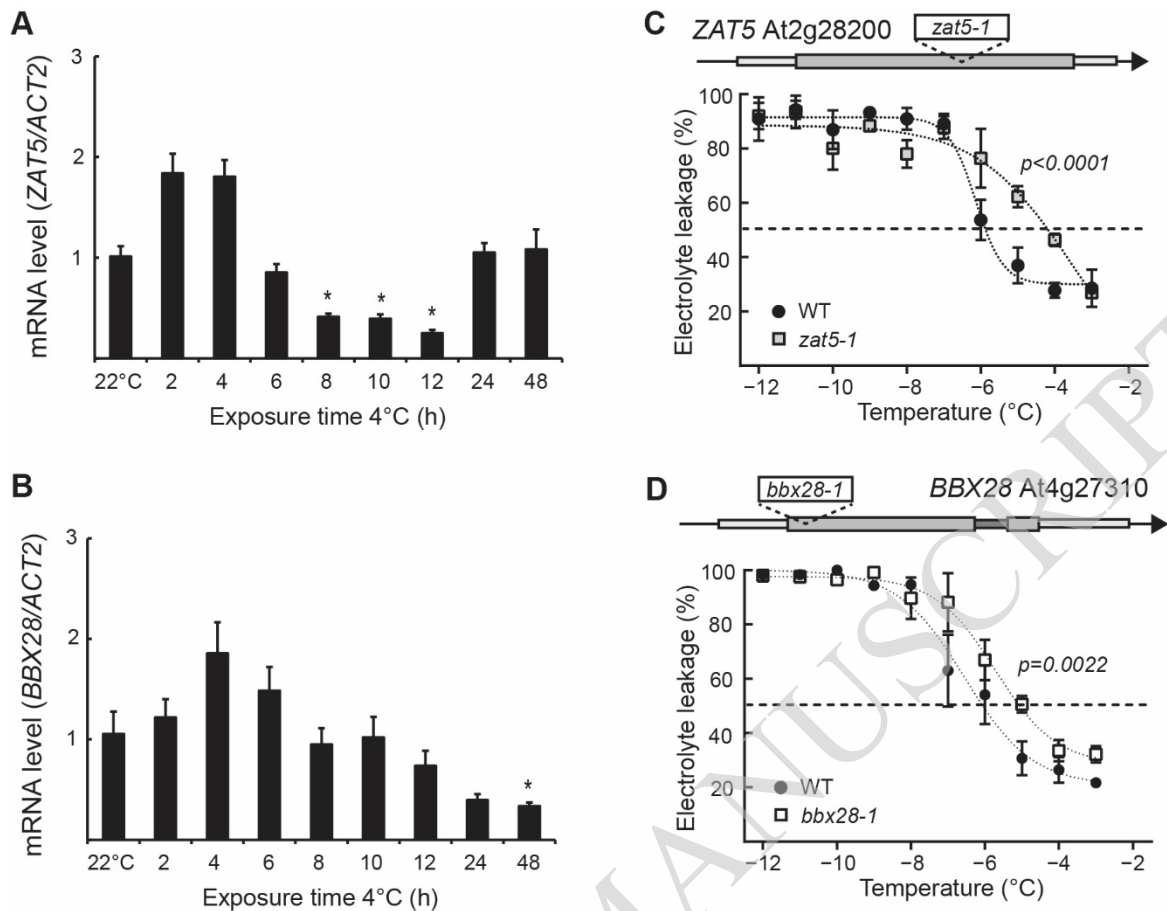


Figure 7. ZAT5 and BBX28 are important for cold acclimation.

A) The relative steady-state level of ZAT5 measured by RT-qPCR following cold exposure (4°C). Steady-state levels were normalized to WT levels at 22°C. The mean values are from three biological replicates. Error bars represent \pm SEM. Statistical significance was calculated with Student's t-test (* $p < 0.05$).

B) The relative steady-state level of BBX28 measured by RT-qPCR following cold exposure (4°C). Steady-state levels were normalized to WT levels at 22°C. The mean values are from three biological replicates. Error bars represent \pm SEM. Statistical significance was calculated with Student's t-test (* $p < 0.05$).

C) Electrolyte leakage in wild-type and *zat5-1* of cold-acclimated (4 days of 4°C) plants. Each data point represents the mean from at least 3 biological replicates (\pm SEM). The dashed line represents the threshold value, 50%. The dotted lines represent the curve fit. Statistical significance was calculated with an extra sum-of-squares F test and the p value is shown in the figure.

D) Electrolyte leakage in wild-type and *bbx28-1* of cold-acclimated (4 days of 4°C) plants. Each data point represents the mean from at least 3 biological replicates (\pm SEM). The dashed line represents the threshold value, 50%. The dotted lines represent the curve fit. Statistical significance was calculated with an extra sum-of-squares F test and the p value is shown in the figure.

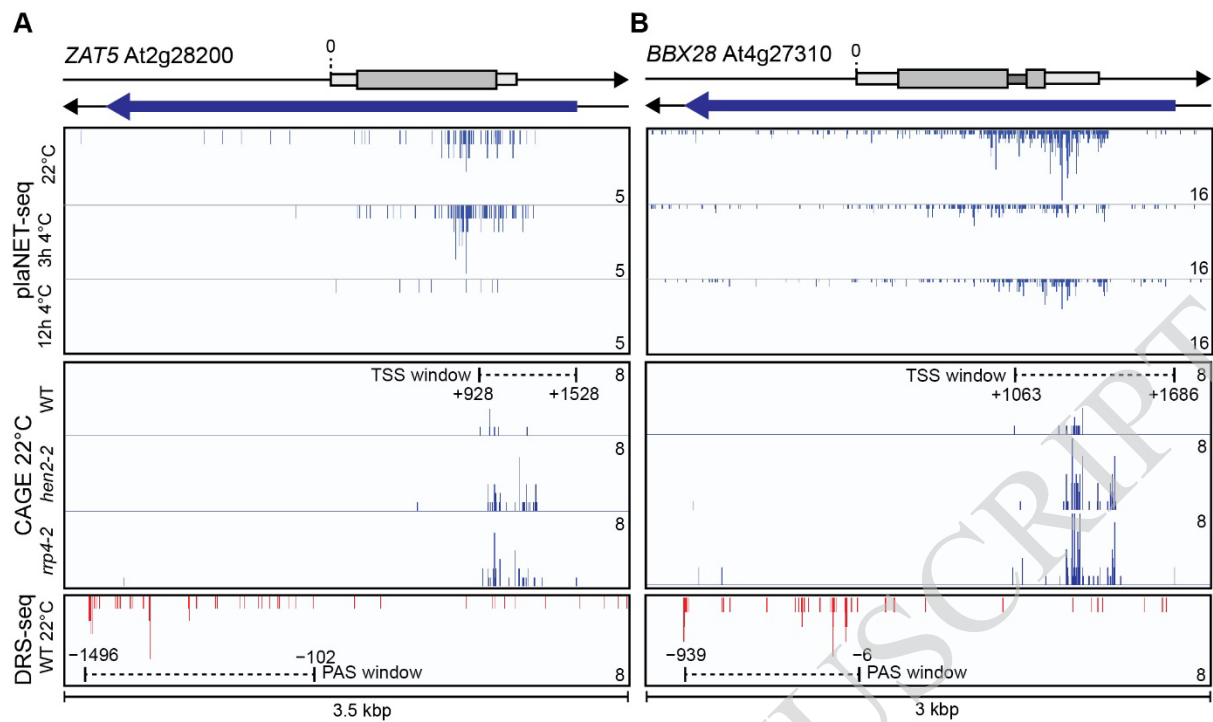


Figure 8. Characterization of *asZAT5* and *asBBX28*.

Screenshots from plaNET-seq (upper panel), CAGE (middle panel), and DRS-seq (lower panel) for **A)** *ZAT5*, and **B)** *BBX28*. 0 indicates the TSS of the sense transcript. Elevated transcriptional activity indicated by higher peaks density and amplitude.

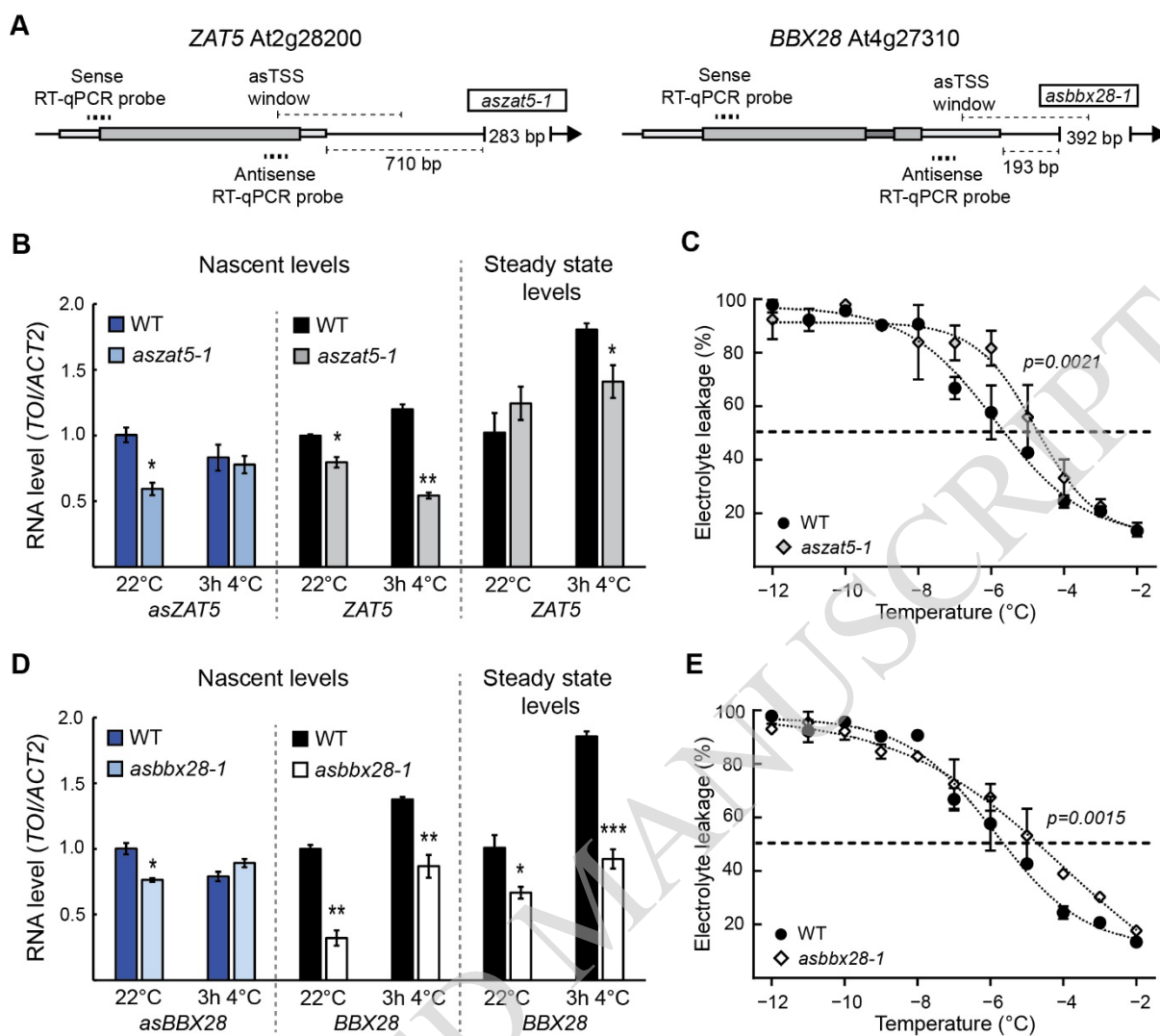


Figure 9. *asZAT5* and *asBBX28* are important for proper regulation of their host gene.

A) Graphical representation of the *ZAT5* and the *BBX28* loci showing the location of sequence targeted by CRISPR-Cas9 to generate an *asZAT5* knockdown line (*aszat5-1*) and an *asBBX28* knockdown line (*asbbx28-1*). Antisense transcription start site (asTSS) window and distances of knocked out genomic sequence from 3'-end are marked with dotted lines. Location of RT-qPCR probes for sense and antisense are shown.

B) The relative nascent and steady-state level of *asZAT5* and *ZAT5* in wild-type and *aszat5-1* measured by RT-qPCR at 22°C and following 3h of cold exposure (4°C). All levels were normalized to WT levels at 22°C. The mean values are from three biological replicates. Error bars represent \pm SEM. Statistical significance was calculated with Student's t-test (* $p < 0.05$).

C) Electrolyte leakage in wild-type and *aszat5-1* of cold-acclimated (5 days of 4°C) plants. Each data point represents the mean from at least 3 biological replicates (\pm SEM). The dashed line represents the threshold value, 50%. The dotted lines represent the curve fit. Statistical significance was calculated with an extra sum-of-squares F test and the p value is shown in the figure.

D) The relative steady-state level of *asBBX28* and *BBX28* in wild-type and *asbbx28-1* measured by RT-qPCR at 22°C and following 3h of cold exposure (4°C). All levels were normalized to WT levels at 22°C. The mean values are from three biological replicates. Error bars represent \pm SEM. Statistical significance was calculated with Student's t-test (* $p < 0.05$).

E) Electrolyte leakage in wild-type and *asbbx28-1* of cold-acclimated (5 days of 4°C) plants. Each data point represents the mean from at least 3 biological replicates (\pm SEM). The dashed line represents the threshold value, 50%. The dotted lines represent the curve fit. Statistical significance was calculated with an extra sum-of-squares F test and the p value is shown in the figure.

ACCEPTED MANUSCRIPT

Parsed Citations

Archacki, R., Yatusевич, R., Buszewicz, D., Krzyczmonik, K., Patryn, J., Iwanicka-Nowicka, R., Biecek, P., Wilczynski, B., Koblowska, M., Jerzmanowski, A., and Swiezewski, S. (2017). Arabidopsis SWM/SNF chromatin remodeling complex binds both promoters and terminators to regulate gene expression. *Nucleic Acids Res* 45, 3116-3129.

Google Scholar: [Author Only](#) [Title Only](#) [Author and Title](#)

Ariel, F., Jegu, T., Latrassé, D., Romero-Barríos, N., Christ, A., Benhamed, M., and Crespi, M. (2014). Noncoding Transcription by Alternative RNA Polymerases Dynamically Regulates an Auxin-Driven Chromatin Loop. *Molecular Cell* 55, 383-396.

Google Scholar: [Author Only](#) [Title Only](#) [Author and Title](#)

Ariel, F., Lucero, L., Christ, A., Mammarella, M.F., Jegu, T., Veluchamy, A., Mariappan, K., Latrassé, D., Blein, T., Liu, C., Benhamed, M., and Crespi, M. (2020). R-Loop Mediated trans Action of the APOLO Long Noncoding RNA. *Molecular Cell* 77, 1055-1065.e1054.

Google Scholar: [Author Only](#) [Title Only](#) [Author and Title](#)

Bolger, A.M., Lohse, M., and Usadel, B. (2014). Trimmomatic: a flexible trimmer for Illumina sequence data. *Bioinformatics* 30, 2114-2120.

Google Scholar: [Author Only](#) [Title Only](#) [Author and Title](#)

Borsani, O., Zhu, J., Verslues, P.E., Sunkar, R., and Zhu, J.-K. (2005). Endogenous siRNAs Derived from a Pair of Natural cis-Antisense Transcripts Regulate Salt Tolerance in Arabidopsis. *Cell* 123, 1279-1291.

Google Scholar: [Author Only](#) [Title Only](#) [Author and Title](#)

Brown, T., Howe, F.S., Murray, S.C., Wouters, M., Lorenz, P., Seward, E., Rata, S., Angel, A., and Mellor, J. (2018). Antisense transcription-dependent chromatin signature modulates sense transcript dynamics. *Molecular Systems Biology* 14, e8007.

Google Scholar: [Author Only](#) [Title Only](#) [Author and Title](#)

Cao, J., Liang, Y., Yan, T., Wang, X., Zhou, H., Chen, C., Zhang, Y., Zhang, B., Zhang, S., Liao, J., Cheng, S., Chu, J., Huang, X., Xu, D., Li, J., Deng, X.W., and Lin, F. (2022). The photomorphogenic repressors BBX28 and BBX29 integrate light and brassinosteroid signaling to inhibit seedling development in Arabidopsis. *Plant Cell* 34, 2266-2285.

Google Scholar: [Author Only](#) [Title Only](#) [Author and Title](#)

Chen, M.-X., Zhu, F.-Y., Gao, B., Ma, K.-L., Zhang, Y., Fernie, A.R., Chen, X., Dai, L., Ye, N.-H., Zhang, X., Tian, Y., Zhang, D., Xiao, S., Zhang, J., and Liu, Y.-G. (2019). Full-Length Transcript-Based Proteogenomics of Rice Improves Its Genome and Proteome Annotation1. *Plant Physiology* 182, 1510-1526.

Google Scholar: [Author Only](#) [Title Only](#) [Author and Title](#)

Chiba, Y., Mineta, K., Hirai, M.Y., Suzuki, Y., Kanaya, S., Takahashi, H., Onouchi, H., Yamaguchi, J., and Naito, S. (2012). Changes in mRNA Stability Associated with Cold Stress in Arabidopsis Cells. *Plant and Cell Physiology* 54, 180-194.

Google Scholar: [Author Only](#) [Title Only](#) [Author and Title](#)

Csorba, T., Questa, J.I., Sun, Q., and Dean, C. (2014). Antisense COOLAIR mediates the coordinated switching of chromatin states at FLC during vernalization. *Proceedings of the National Academy of Sciences* 111, 16160-16165.

Google Scholar: [Author Only](#) [Title Only](#) [Author and Title](#)

Delhomme, N., Zare, A., Shutava, I., Kochakarn, T.F., Mähler, N., Serrano, A., Irani-Shemirani, M., and Evanzalen. (2023). UPSCb/UPSCb-common: Release as of 15th December 2023 (Version v20231215). Zenodo.

Google Scholar: [Author Only](#) [Title Only](#) [Author and Title](#)

Ding, Y., Virilouvet, L., Liu, N., Riethoven, J.-J., Fromm, M., and Avramova, Z. (2014). Dehydration stress memory genes of *Zea mays*; comparison with *Arabidopsis thaliana*. *BMC Plant Biology* 14, 141.

Google Scholar: [Author Only](#) [Title Only](#) [Author and Title](#)

Dobin, A., Davis, C.A., Schlesinger, F., Drenkow, J., Zaleski, C., Jha, S., Batut, P., Chaisson, M., and Gingeras, T.R. (2012). STAR: ultrafast universal RNA-seq aligner. *Bioinformatics* 29, 15-21.

Google Scholar: [Author Only](#) [Title Only](#) [Author and Title](#)

Fedak, H., Palusinska, M., Krzyczmonik, K., Brzezniak, L., Yatusевич, R., Pietras, Z., Kaczanowski, S., and Swiezewski, S. (2016). Control of seed dormancy in Arabidopsis by a cis-acting noncoding antisense transcript. *Proceedings of the National Academy of Sciences* 113, E7846-E7855.

Google Scholar: [Author Only](#) [Title Only](#) [Author and Title](#)

Held, M.A., Penning, B., Brandt, A.S., Kessans, S.A., Yong, W., Scofield, S.R., and Carpita, N.C. (2008). Small-interfering RNAs from natural antisense transcripts derived from a cellulose synthase gene modulate cell wall biosynthesis in barley. *Proceedings of the National Academy of Sciences* 105, 20534-20539.

Google Scholar: [Author Only](#) [Title Only](#) [Author and Title](#)

Henriques, R., Wang, H., Liu, J., Boix, M., Huang, L.F., and Chua, N.H. (2017). The antiphasic regulatory module comprising CDF5 and its antisense RNA FLORE links the circadian clock to photoperiodic flowering. *New Phytol* 216, 854-867.

Google Scholar: [Author Only](#) [Title Only](#) [Author and Title](#)

Henz, S.R., Cumbie, J.S., Kasschau, K.D., Lohmann, J.U., Carrington, J.C., Weigel, D., and Schmid, M. (2007). Distinct Expression Patterns of Natural Antisense Transcripts in Arabidopsis. *Plant Physiology* 144, 1247-1255.

Google Scholar: [Author Only](#) [Title Only](#) [Author and Title](#)

Jabnourne, M., Secco, D., Lecampion, C., Robaglia, C., Shu, Q., and Poirier, Y. (2013). A rice cis-natural antisense RNA acts as a translational enhancer for its cognate mRNA and contributes to phosphate homeostasis and plant fitness. *Plant Cell* 25, 4166-4182.

Google Scholar: [Author Only](#) [Title Only](#) [Author and Title](#)

Katiyar-Agarwal, S., Morgan, R., Dahlbeck, D., Borsani, O., Villegas, A., Zhu, J.-K., Staskawicz, B.J., and Jin, H. (2006). A pathogen-inducible endogenous siRNA in plant immunity. *Proceedings of the National Academy of Sciences* 103, 18002-18007.

Google Scholar: [Author Only](#) [Title Only](#) [Author and Title](#)

Kent, W.J., Zweig, A.S., Barber, G., Hinrichs, A.S., and Karolchik, D. (2010). BigWig and BigBed: enabling browsing of large distributed datasets. *Bioinformatics* 26, 2204-2207.

Google Scholar: [Author Only](#) [Title Only](#) [Author and Title](#)

Kindgren, P., Dubreuil, C., and Strand, Å. (2015). The Recovery of Plastid Function Is Required for Optimal Response to Low Temperatures in Arabidopsis. *PLOS ONE* 10, e0138010.

Google Scholar: [Author Only](#) [Title Only](#) [Author and Title](#)

Kindgren, P., Ivanov, M., and Marquardt, S. (2019). Native elongation transcript sequencing reveals temperature dependent dynamics of nascent RNAPII transcription in Arabidopsis. *Nucleic Acids Research* 48, 2332-2347.

Google Scholar: [Author Only](#) [Title Only](#) [Author and Title](#)

Kindgren, P., Ard, R., Ivanov, M., and Marquardt, S. (2018). Transcriptional read-through of the long non-coding RNA SVALKA governs plant cold acclimation. *Nature Communications* 9, 4561.

Google Scholar: [Author Only](#) [Title Only](#) [Author and Title](#)

Kopylova, E., Noé, L., and Touzet, H. (2012). SortMeRNA: fast and accurate filtering of ribosomal RNAs in metatranscriptomic data. *Bioinformatics* 28, 3211-3217.

Google Scholar: [Author Only](#) [Title Only](#) [Author and Title](#)

Lampropoulos, A., Sutikovic, Z., Wenzl, C., Maegele, I., Lohmann, J.U., and Forner, J. (2013). GreenGate---a novel, versatile, and efficient cloning system for plant transgenesis. *PLoS One* 8, e83043.

Google Scholar: [Author Only](#) [Title Only](#) [Author and Title](#)

Lange, H., Zuber, H., Sement, F.M., Chicher, J., Kuhn, L., Hammann, P., Brunaud, V., Bérard, C., Bouteiller, N., Balzergue, S., Aubourg, S., Martin-Magniette, M.-L., Vaucheret, H., and Gagliardi, D. (2014). The RNA Helicases AtMTR4 and HEN2 Target Specific Subsets of Nuclear Transcripts for Degradation by the Nuclear Exosome in Arabidopsis thaliana. *PLOS Genetics* 10, e1004564.

Google Scholar: [Author Only](#) [Title Only](#) [Author and Title](#)

Li, C., Gu, L., Gao, L., Chen, C., Wei, C.-Q., Qiu, Q., Chien, C.-W., Wang, S., Jiang, L., Ai, L.-F., Chen, C.-Y., Yang, S., Nguyen, V., Qi, Y., Snyder, M.P., Burlingame, A.L., Kohalmi, S.E., Huang, S., Cao, X., Wang, Z.-Y., Wu, K., Chen, X., and Cui, Y. (2016). Concerted genomic targeting of H3K27 demethylase REF6 and chromatin-remodeling ATPase BRM in Arabidopsis. *Nature Genetics* 48, 687-693.

Google Scholar: [Author Only](#) [Title Only](#) [Author and Title](#)

Li, X., Yang, Q., Liao, X., Tian, Y., Zhang, F., Zhang, L., and Liu, Q. (2022). A natural antisense RNA improves chrysanthemum cold tolerance by regulating the transcription factor DgTCP1. *Plant Physiology*.

Google Scholar: [Author Only](#) [Title Only](#) [Author and Title](#)

Liu, C., Xin, Y., Xu, L., Cai, Z., Xue, Y., Liu, Y., Xie, D., Liu, Y., and Qi, Y. (2018). Arabidopsis ARGONAUTE 1 Binds Chromatin to Promote Gene Transcription in Response to Hormones and Stresses. *Developmental Cell* 44, 348-361.e347.

Google Scholar: [Author Only](#) [Title Only](#) [Author and Title](#)

Liu, M., Zhu, J., and Dong, Z. (2021). Immediate transcriptional responses of Arabidopsis leaves to heat shock. *Journal of Integrative Plant Biology* 63, 468-483.

Google Scholar: [Author Only](#) [Title Only](#) [Author and Title](#)

Love, M.I., Huber, W., and Anders, S. (2014). Moderated estimation of fold change and dispersion for RNA-seq data with DESeq2. *Genome Biology* 15, 550.

Google Scholar: [Author Only](#) [Title Only](#) [Author and Title](#)

Lucero, L., Ferrero, L., Fonouni-Farde, C., and Ariel, F. (2021). Functional classification of plant long noncoding RNAs: a transcript is known by the company it keeps. *New Phytologist* 229, 1251-1260.

Google Scholar: [Author Only](#) [Title Only](#) [Author and Title](#)

Mao, Y.S., Sunwoo, H., Zhang, B., and Spector, D.L. (2011). Direct visualization of the co-transcriptional assembly of a nuclear

body by noncoding RNAs. *Nature Cell Biology* 13, 95-101.

Google Scholar: [Author Only](#) [Title Only](#) [Author and Title](#)

Marquis, V., Smirnova, E., Graindorge, S., Delcros, P., Villette, C., Zumsteg, J., Heintz, D., and Heitz, T. (2022). Broad-spectrum stress tolerance conferred by suppressing jasmonate signaling attenuation in *Arabidopsis* JASMONIC ACID OXIDASE mutants. *The Plant Journal* 109, 856-872.

Google Scholar: [Author Only](#) [Title Only](#) [Author and Title](#)

Matsui, A., Ishida, J., Morosawa, T., Mochizuki, Y., Kaminuma, E., Endo, T.A., Okamoto, M., Nambara, E., Nakajima, M., Kawashima, M., Satou, M., Kim, J.-M., Kobayashi, N., Toyoda, T., Shinozaki, K., and Seki, M. (2008). *Arabidopsis* Transcriptome Analysis under Drought, Cold, High-Salinity and ABA Treatment Conditions using a Tiling Array. *Plant and Cell Physiology* 49, 1135-1149.

Google Scholar: [Author Only](#) [Title Only](#) [Author and Title](#)

Mayer, A., di Iulio, J., Maleri, S., Eser, U., Vierstra, J., Reynolds, A., Sandstrom, R., Stamatoyannopoulos, John A., and Churchman, L.S. (2015). Native Elongating Transcript Sequencing Reveals Human Transcriptional Activity at Nucleotide Resolution. *Cell* 161, 541-554.

Google Scholar: [Author Only](#) [Title Only](#) [Author and Title](#)

Murray, S.C., Haenni, S., Howe, F.S., Fischl, H., Chocian, K., Nair, A., and Mellor, J. (2015). Sense and antisense transcription are associated with distinct chromatin architectures across genes. *Nucleic Acids Research* 43, 7823-7837.

Google Scholar: [Author Only](#) [Title Only](#) [Author and Title](#)

Narsai, R., Howell, K.A., Millar, A.H., O'Toole, N., Small, I., and Whelan, J. (2007). Genome-Wide Analysis of mRNA Decay Rates and Their Determinants in *Arabidopsis thaliana*. *Plant Cell* 19, 3418-3436.

Google Scholar: [Author Only](#) [Title Only](#) [Author and Title](#)

Nielsen, M., Ard, R., Leng, X., Ivanov, M., Kindgren, P., Pelechano, V., and Marquardt, S. (2019). Transcription-driven chromatin repression of intragenic transcription start sites. *PLOS Genetics* 15, e1007969.

Google Scholar: [Author Only](#) [Title Only](#) [Author and Title](#)

Parent, J.-S., Jauvion, V., Bouché, N., Béclin, C., Hachet, M., Zytnicki, M., and Vaucheret, H. (2015). Post-transcriptional gene silencing triggered by sense transgenes involves uncapped antisense RNA and differs from silencing intentionally triggered by antisense transgenes. *Nucleic Acids Research* 43, 8464-8475.

Google Scholar: [Author Only](#) [Title Only](#) [Author and Title](#)

Patro, R., Duggal, G., Love, M.I., Irizarry, R.A., and Kingsford, C. (2017). Salmon provides fast and bias-aware quantification of transcript expression. *Nature Methods* 14, 417-419.

Google Scholar: [Author Only](#) [Title Only](#) [Author and Title](#)

Perea-Resa, C., Hernández-Verdeja, T., López-Cobollo, R., Castellano, M.d.M., and Salinas, J. (2012). LSM Proteins Provide Accurate Splicing and Decay of Selected Transcripts to Ensure Normal *Arabidopsis* Development. *Plant Cell* 24, 4930-4947.

Google Scholar: [Author Only](#) [Title Only](#) [Author and Title](#)

Ramírez, F., Ryan, D.P., Grüning, B., Bhardwaj, V., Kilpert, F., Richter, A.S., Heyne, S., Dündar, F., and Manke, T. (2016). deepTools2: a next generation web server for deep-sequencing data analysis. *Nucleic Acids Research* 44, W160-W165.

Google Scholar: [Author Only](#) [Title Only](#) [Author and Title](#)

Reis, R.S., and Poirier, Y. (2021). Making sense of the natural antisense transcript puzzle. *Trends in Plant Science* 26, 1104-1115.

Google Scholar: [Author Only](#) [Title Only](#) [Author and Title](#)

Romanowski, A., Schlaen, R.G., Perez-Santangelo, S., Mancini, E., and Yanovsky, M.J. (2020). Global transcriptome analysis reveals circadian control of splicing events in *Arabidopsis thaliana*. *The Plant Journal* 103, 889-902.

Google Scholar: [Author Only](#) [Title Only](#) [Author and Title](#)

Roulé, T., Christ, A., Hussain, N., Huang, Y., Hartmann, C., Benhamed, M., Gutierrez-Marcos, J., Ariel, F., Crespi, M., and Blein, T. (2022). The lncRNA MARS modulates the epigenetic reprogramming of the marneral cluster in response to ABA. *Molecular Plant* 15, 840-856.

Google Scholar: [Author Only](#) [Title Only](#) [Author and Title](#)

Schurch, N.J., Cole, C., Sherstnev, A., Song, J., Duc, C., Storey, K.G., McLean, W.H.I., Brown, S.J., Simpson, G.G., and Barton, G.J. (2014). Improved Annotation of 3' Untranslated Regions and Complex Loci by Combination of Strand-Specific Direct RNA Sequencing, RNA-Seq and ESTs. *PLOS ONE* 9, e94270.

Google Scholar: [Author Only](#) [Title Only](#) [Author and Title](#)

Shen, L., Shao, N., Liu, X., and Nestler, E. (2014). ngs.plot: Quick mining and visualization of next-generation sequencing data by integrating genomic databases. *BMC Genomics* 15, 284.

Google Scholar: [Author Only](#) [Title Only](#) [Author and Title](#)

Sidaway-Lee, K., Costa, M.J., Rand, D.A., Finkenstadt, B., and Penfield, S. (2014). Direct measurement of transcription rates reveals multiple mechanisms for configuration of the *Arabidopsis* ambient temperature response. *Genome Biology* 15, R45.

Google Scholar: [Author Only](#) [Title Only](#) [Author and Title](#)

Song, Z., Yan, T., Liu, J., Bian, Y., Heng, Y., Lin, F., Jiang, Y., Wang Deng, X., and Xu, D. (2020). BBX28/BBX29, HY5 and BBX30/31 form a feedback loop to fine-tune photomorphogenic development. *The Plant Journal* 104, 377-390.

Google Scholar: [Author Only](#) [Title Only](#) [Author and Title](#)

Sorenson, R.S., Deshotel, M.J., Johnson, K., Adler, F.R., and Sieburth, L.E. (2018). Arabidopsis mRNA decay landscape arises from specialized RNA decay substrates, decapping-mediated feedback, and redundancy. *Proceedings of the National Academy of Sciences* 115, E1485-E1494.

Google Scholar: [Author Only](#) [Title Only](#) [Author and Title](#)

Swiezewski, S., Liu, F., Magusin, A., and Dean, C. (2009). Cold-induced silencing by long antisense transcripts of an Arabidopsis Polycomb target. *Nature* 462, 799-802.

Google Scholar: [Author Only](#) [Title Only](#) [Author and Title](#)

Swiezewski, S., Crevillen, P., Liu, F., Ecker, J.R., Jermanski, A., and Dean, C. (2007). Small RNA-mediated chromatin silencing directed to the 3' region of the Arabidopsis gene encoding the developmental regulator, FLC. *Proceedings of the National Academy of Sciences* 104, 3633-3638.

Google Scholar: [Author Only](#) [Title Only](#) [Author and Title](#)

Thieffry, A., Vigh, M.L., Bornholdt, J., Ivanov, M., Brodersen, P., and Sandelin, A. (2020). Characterization of Arabidopsis thaliana Promoter Bidirectionality and Antisense RNAs by Inactivation of Nuclear RNA Decay Pathways. *Plant Cell* 32, 1845-1867.

Google Scholar: [Author Only](#) [Title Only](#) [Author and Title](#)

Wan, Q., Guan, X., Yang, N., Wu, H., Pan, M., Liu, B., Fang, L., Yang, S., Hu, Y., Ye, W., Zhang, H., Ma, P., Chen, J., Wang, Q., Mei, G., Cai, C., Yang, D., Wang, J., Guo, W., Zhang, W., Chen, X., and Zhang, T. (2016). Small interfering RNAs from bidirectional transcripts of GhMML3_A12 regulate cotton fiber development. *New Phytologist* 210, 1298-1310.

Google Scholar: [Author Only](#) [Title Only](#) [Author and Title](#)

Wang, H., Chung, P.J., Liu, J., Jang, I.-C., Kean, M.J., Xu, J., and Chua, N.-H. (2014). Genome-wide identification of long noncoding natural antisense transcripts and their responses to light in Arabidopsis. *Genome Research* 24, 444-453.

Google Scholar: [Author Only](#) [Title Only](#) [Author and Title](#)

Wang, H., Zhang, Z., Li, H., Zhao, X., Liu, X., Ortiz, M., Lin, C., and Liu, B. (2013). CONSTANS-LIKE 7 regulates branching and shade avoidance response in Arabidopsis. *Journal of Experimental Botany* 64, 1017-1024.

Google Scholar: [Author Only](#) [Title Only](#) [Author and Title](#)

Wierzbicki, A.T., Blevins, T., and Swiezewski, S. (2021). Long Noncoding RNAs in Plants. *Annual Review of Plant Biology* 72, 245-271.

Google Scholar: [Author Only](#) [Title Only](#) [Author and Title](#)

Wu, H.-W., Deng, S., Xu, H., Mao, H.-Z., Liu, J., Niu, Q.-W., Wang, H., and Chua, N.-H. (2018). A noncoding RNA transcribed from the AGAMOUS (AG) second intron binds to CURLY LEAF and represses AG expression in leaves. *New Phytologist* 219, 1480-1491.

Google Scholar: [Author Only](#) [Title Only](#) [Author and Title](#)

Xing, D.-H., Lai, Z.-B., Zheng, Z.-Y., Vinod, K.M., Fan, B.-F., and Chen, Z.-X. (2008). Stress- and Pathogen-Induced Arabidopsis WRKY48 is a Transcriptional Activator that Represses Plant Basal Defense. *Molecular Plant* 1, 459-470.

Google Scholar: [Author Only](#) [Title Only](#) [Author and Title](#)

Xing, H.-L., Dong, L., Wang, Z.-P., Zhang, H.-Y., Han, C.-Y., Liu, B., Wang, X.-C., and Chen, Q.-J. (2014). A CRISPR/Cas9 toolkit for multiplex genome editing in plants. *BMC Plant Biology* 14, 327.

Google Scholar: [Author Only](#) [Title Only](#) [Author and Title](#)

Zacharaki, V., Meena, S.K., and Kindgren, P. (2023). The non-coding RNA SVALKA locus produces a cis-natural antisense transcript that negatively regulates the expression of CBF1 and biomass production at normal temperatures. *Plant Communications* 4, 100551.

Google Scholar: [Author Only](#) [Title Only](#) [Author and Title](#)

Zhao, X., Li, J., Lian, B., Gu, H., Li, Y., and Qi, Y. (2018). Global identification of Arabidopsis lncRNAs reveals the regulation of MAF4 by a natural antisense RNA. *Nature Communications* 9, 5056.

Google Scholar: [Author Only](#) [Title Only](#) [Author and Title](#)

Zhu, J., Liu, M., Liu, X., and Dong, Z. (2018). RNA polymerase II activity revealed by GRO-seq and pNET-seq in Arabidopsis. *Nature Plants* 4, 1112-1123.

Google Scholar: [Author Only](#) [Title Only](#) [Author and Title](#)